ECONOMIC GEOLOGY RESEARCH INSTITUTE

University of the Witwatersrand
Johannesburg

— • —

METAMORPHISM OF THE GRANITE-GREENSTONE TERRANE SOUTH OF THE BARBERTON GREENSTONE BELT, SOUTH AFRICA: AN INSIGHT INTO THE TECTONO-THERMAL EVOLUTION OF THE LOWER PORTIONS OF THE ONVERWACHT GROUP

A. DZIGGEL, G. STEVENS, M. POUJOL,
C. R. ANHAEUSSER and R. A. ARMSTRONG

UNIVERSITY OF THE WITWATERSRAND
JOHANNESBURG

METAMORPHISM OF THE GRANITE-GREENSTONE TERRANE SOUTH OF THE BARBERTON GREENSTONE BELT, SOUTH AFRICA: AN INSIGHT INTO THE TECTONO-THERMAL EVOLUTION OF THE LOWER PORTIONS OF THE ONVERWACHT GROUP

by

A. DZIGGEL[a], G. STEVENS[b], M. POUJOL[c], C. R. ANHAEUSSER[a]
and R. A. ARMSTRONG[d]

([a] Economic Geology Research Institute, University of the Witwatersrand, Private Bag 3, PO WITS 2050, Johannesburg, South Africa
[b] Department of Geology, University of Stellenbosch, Matieland, 7140, Stellenbosch, South Africa
[c] Economic Geology Research Institute/Hugh Allsopp Laboratory, Private Bag 3, PO WITS 2050, Johannesburg, South Africa
[d] Research School of Earth Sciences, Australian National University, Canberra, ACT 0200, Australia)

METAMORPHISM OF THE GRANITE-GREENSTONE TERRANE SOUTH OF THE BARBERTON GREENSTONE BELT, SOUTH AFRICA: AN INSIGHT INTO THE TECTONO-THERMAL EVOLUTION OF THE LOWER PORTIONS OF THE ONVERWACHT GROUP

ABSTRACT

Numerous greenstone remnants occur in the granitoid-dominated terrane to the south of the Barberton greenstone belt. These have generally been regarded as part of the lowermost formations of the Onverwacht Group on the basis of lithological correlations and the contact relationships with the intrusive Stolzburg trondhjemite pluton. The greenstone remnants consist of metamorphosed mafic and ultramafic metavolcanic sequences, with associated minor sedimentary units. The sediments consist of thin chert and banded iron formation layers that are interbanded with the cyclic (ultra) mafic volcanic units, as well as an up to 10m-thick clastic sedimentary unit that contains well-preserved primary sedimentary features such as trough cross-bedding. Coarse-grained portions of these metasediments are moderately metamorphosed impure arkoses consisting mainly of quartz, microcline, plagioclase and diopside and which contain up to 4.5 wt% K_2O. SHRIMP ion microprobe and conventional U-Pb dating of detrital zircons reveal ages at 3536, 3526, 3479 and 3442 Ma, respectively, indicating that two protoliths for these sediments predate the formation of the bulk of the Barberton greenstone belt. The oldest age estimate is identical to an age reported for a tectonic wedge of tonalitic gneiss within the Theespruit Formation from the southern portion of the greenstone belt. A minimum age of 3431 11 Ma for the formation of the metasediments is given by a trondhjemite gneiss that locally intrudes the greenstone remnant. Thus, these metasediments were deposited between *c.* 3442 and 3431 Ma, contemporaneously with erosion of spatially associated older granitoid rocks. Portions of the clastic metasediments that are quartz-bearing, but not quartz-rich, show well-defined thin wavy bedding and compositional banding. In these areas the peak-metamorphic mineral assemblage is commonly diopside + andesine + garnet + quartz, with a garnet core composition of Xgrss = 0.60, Xalm = 0.319, Xpyp = 0.023 and Xspss = 0.06. This assemblage, and garnet in particular, is extensively replaced by epidote. Peak metamorphic mineral assemblages of magnesio-hornblende + andesine + quartz, and quartz + ferrosilite + magnetite + grunerite have been recorded from adjacent amphibolites and interlayered iron formation units, respectively. Retrogression is marked by actinolitic rims around peak metamorphic magnesio-hornblende cores in the metamafic rocks, and by a second generation of grunerite that occurs as fibrous aggregates rimming orthopyroxene in the iron formation. Average P-T calculations for the peak-metamorphic mineral assemblages in all these rock types vary between 650-700ºC and 7.0-11.0 kbar. This implies a tectonic setting comparable to some modern orogenic belts and that the granite-greenstone terrane investigated in this study possibly represents an exhumed terrane that formed a basement to the Barberton greenstone belt at the time of the peak metamorphic event. The age of the amphibolite facies metamorphism of rocks correlated with the Fig Tree Group from the Schapenburg schist belt further south is *c.* 3230 Ma. The continuation of the tectonic fabric from Schapenburg into the greenstone remnants investigated in this study suggests that the rocks in both these areas may be recording the mid- to lower-crustal response to the main compressional event in the Barberton area at *c.* 3230 Ma.

———————————**oOo**———————————

METAMORPHISM OF THE GRANITE-GREENSTONE TERRANE SOUTH OF THE BARBERTON GREENSTONE BELT, SOUTH AFRICA: AN INSIGHT INTO THE TECTONO-THERMAL EVOLUTION OF THE LOWER PORTIONS OF THE ONVERWACHT GROUP

CONTENTS

_____oOo_____

METAMORPHISM OF THE GRANITE-GREENSTONE TERRANE SOUTH OF THE BARBERTON GREENSTONE BELT, SOUTH AFRICA: AN INSIGHT INTO THE TECTONO-THERMAL EVOLUTION OF THE LOWER PORTIONS OF THE ONVERWACHT GROUP

INTRODUCTION

The *c.* 3550-3200 Ma Barberton greenstone belt in South Africa (Fig. 1) is regarded as one of the best preserved, early Archaean supracrustal sequences on Earth. The greenstone sequence has been subdivided into a lowermost Onverwacht Group that is dominated by mafic and ultramafic volcanic rocks; an overlying Fig Tree Group, consisting of pelagic sediments and intermediate composition extrusive rocks; and, an upper Moodies Group, predominately consisting of arenaceous clastic sediments. Together, these units constitute the Swaziland Supergroup (Anhaeusser, 1975; Lowe and Byerly, 1999). Early views of the geology of the greenstone belt saw the entire 25km-thick stratigraphic sequence as a continuous volcano-sedimentary succession (Viljoen and Viljoen, 1969; Anhaeusser, 1975). Furthermore, the largely subvertical orientation of the stratigraphy was seen as a consequence of deformation during diapiric intrusion of the tonalitic and trondhjemitic gneiss plutons exposed in contact with the Onverwacht Group rocks from many areas around the belt. Anhaeusser (1973) proposed that these granitoids were derived from the anatexis of portions of the Onverwacht Group that underwent deep burial as a consequence of gravity-driven syncline formation. The intrusion of these primitive granitoids was followed by the post-deformation intrusion of large sheet-like bodies of granodiorite derived from the partial melting of the older tonalitic and trondhjemitic gneisses (Anhaeusser, 1973; Anhaeusser and Robb, 1981,1983; Robb et al., 1983). The magmatic history of the belt was concluded by the intrusion of potassic granites and the Boesmanskop syenite (Anhaeusser and Robb, 1981; Anhaeusser et al., 1983; Robb, 1983a). Thus, felsic plutonism associated with the Barberton greenstone belt was seen as being characterised by successive episodes of intrusion of increasingly chemically evolved magmas. These magmas were derived from the melting of rock types similar to those currently exposed within the belt. Deformation was largely a consequence of the vertical motion of mafic/ultramafic and felsic rock masses relative to one another. In this scenario metamorphism of the greenstone sequence was primarily interpreted as a contact phenomena driven by the intruding granitoids (Anhaeusser, 1973; 1984).

Recent structural and geochronological studies have, however, begun to reveal a complex and polyphase tectono-magmatic history (e.g., de Wit, 1982; Armstrong et al., 1990; de Ronde and de Wit, 1994; Kamo and Davis, 1994; de Ronde and Kamo, 2000), which encompasses a timespan of approximately 400 million years. High-precision single-zircon geochronology has shown that plutonism in the Barberton greenstone belt occurred sporadically, and that the different granitoid types have considerable age overlaps (e.g., Kamo and Davis, 1994; de Ronde and Kamo, 2000; Fig. 1). These studies have also confirmed earlier suggestions that the stratigraphy of the greenstone belt includes major structural breaks and tectonic repetitions (e.g., de Wit, 1982, 1991). The oldest rocks dated so far are felsic schists that have been correlated with the Theespruit Formation exposed in the Steynsdorp anticline (Fig. 1, ~3544 3 to ~3547 3 Ma, Kröner et al., 1996). In this region, rocks of the so-called Theespruit Formation (Viljoen et al., 1969) have been intruded by the *c.* 3509 Ma Steynsdorp pluton (Kamo and Davis, 1994) and both sets of rocks record evidence for a deformation phase that predates the deposition of the bulk of the Onverwacht Group (Kisters and Anhaeusser, 1995a). Thus, the Steynsdorp anticline has been interpreted to represent the oldest nucleus of the belt, onto which the overlying rocks of the Onverwacht Group were tectonically and magmatically accreted (e.g., Kröner et al., 1996; Lowe, 1994, 1999). The next tectono - magmatic episode recorded involved the formation of recumbent nappes and downward- facing sequences in response to horizontal shortening in rocks of the Onverwacht and lower Fig Tree Groups in the southern part of the belt (e.g., de Wit, 1982; de Wit et al., 1987b). It was at this time that the rocks above the Komati fault are thought to have amalgamated with the underlying Theespruit Formation
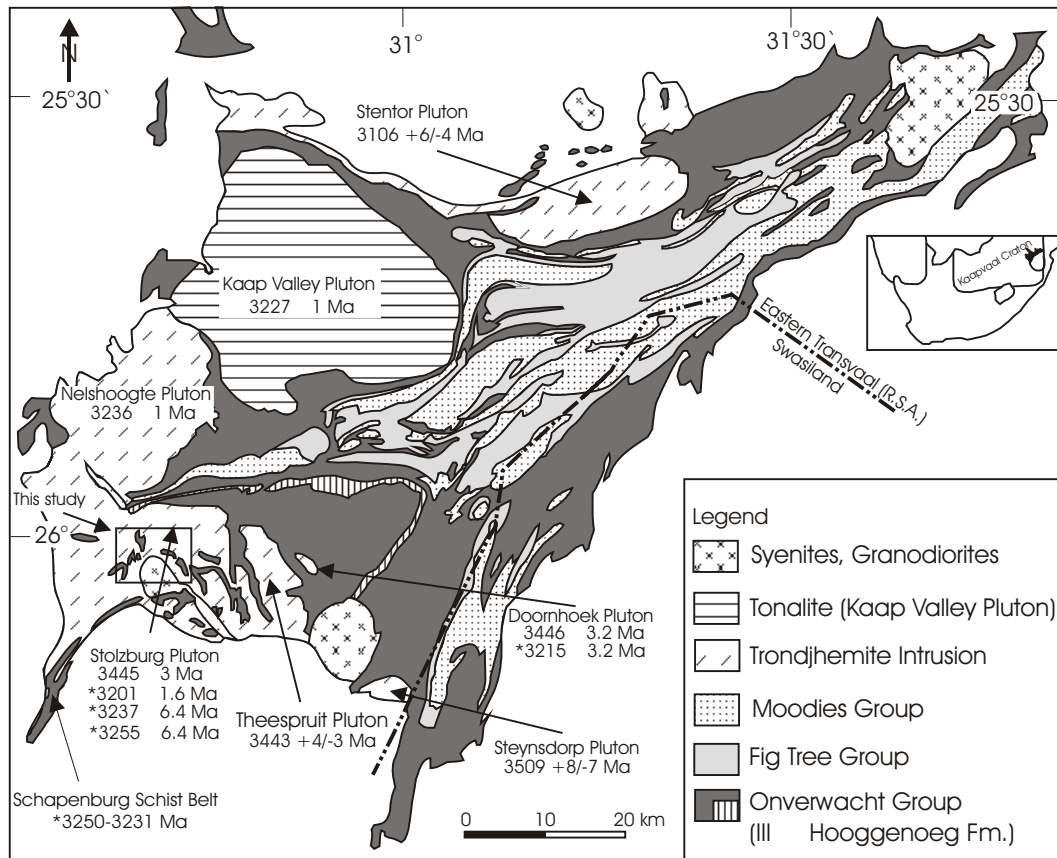
Figure 1: *Simplified geological map of the Barberton greenstone belt, modified after de Ronde and de Wit (1994). Geochronological data are from Kamo and Davis (1994), except for the ages on the Nelshoogte pluton (de Ronde and Kamo, 2000) and the Schapenburg schist belt (Stevens et al., in prep.). Numbers marked with an* are interpreted to be metamorphic ages. All other ages are supposedly intrusive ages.*

(e.g., de Wit, 1991; de Ronde and de Wit, 1994). Deformation was associated with intense calc-alkaline magmatic activity, including the *c*. 3445 Ma trondhjemitic plutonism at the southern margin of the belt and the formation of extrusive felsic equivalents in the Theespruit and Hooggenoeg Formations (e.g., de Wit et al., 1987a; de Ronde and de Wit, 1994). U-Pb and Pb-Pb zircon evaporation ages for the syntectonic felsic intrusions indicate that this early deformation occurred between 3445 and 3416 Ma (e.g., Armstrong et al., 1990; Kröner and Todt, 1988; Kamo and Davis, 1994). The tectonic wedges of the *c*. 3538 Ma tonalitic gneisses preserved in the *c*. 3453 Ma old Theespruit Formation have been used to argue the presence of an older sialic basement (Armstrong et al., 1990). Most of the deformation in the belt is believed to have occurred during a short-lived compressional tectonic event, which coincided with the syndeformational deposition of the upper Fig Tree and Moodies Group sediments and the intrusion of the *c*. 3227 Ma old Kaap Valley tonalite pluton (e.g., Kamo and Davis, 1994). This event was responsible for the upright, tight-to-isoclinal folding, the formation of thrust faults, and eventually, the amalgamation of the northern and southern part of the greenstone belt along the Saddleback-Inyoka fault system (de Ronde and de Wit, 1994). Age estimates on pre- to post-tectonic intrusions in the northern part of the belt indicate that this deformation event occurred over a period of 3 million years, between 3229 Ma and 3226 Ma (Kamo and Davis, 1994; de Ronde and Kamo, 2000). The emplacement of large volumes of sheet-like potassic granites, namely the *c*. 3100 Ma Nelspruit and Mpuluzi batholiths (Anhaeusser and Robb, 1983; Robb et al., 1983a; Kamo and Davis, 1994), marked the final stabilisation of the greenstone belt and its surroundings. The shear-zone-hosted gold mineralisation in the northern part of the belt correlates with this age. Time constraints are given by a *c*. 3126 Ma porphyry dyke predating the shearing and a *c*. 3084 Ma age for hydrothermal rutile associated with

gold at Fairview Mine (de Ronde et al., 1991). It has been suggested that this late-tectonic history of the belt was associated with a change from convergent to transtensional (extensional) tectonics (de Ronde and de Wit, 1994).

As in most other Archaean greenstone belts, the link between deformation, magmatism and metamorphism in the Barberton greenstone belt has not been fully explored. The pervasive greenschist facies metamorphism preserved in the south-central parts of the belt has been interpreted as the result of both seafloor and subsequent burial metamorphism (e.g., Cloete, 1991, 1999; Fig. 2), which correlates in age with the 3450-3490 Ma $^{40}Ar/^{39}Ar$ ages found for some komatiites and komatiitic basalts (Lopez Martinez et al., 1984). The amphibolite facies metamorphism in contact with the surrounding plutons has been suggested by several studies to be a subsequent contact-metamorphic overprint associated with the emplacement of these plutons (e.g., Anheausser, 1969, 1984; Cloete, 1991; Harris et al., 1993). However, metamorphic as well as geochronological data (Kamo and Davis, 1994; Stevens et al., in prep.) indicate that the peak-metamorphic mineral assemblages in some areas equilibrated substantially later than the emplacement of the adjacent plutons, and that some trondhjemite plutons have metamorphic rims on igneous zircons that record metamorphism some 200 Ma younger than the crystallization ages. These authors suggested that a major regional metamorphic event correlates with the main compressional event, and therefore occurred after the deposition of the Fig Tree and overlying Moodies Groups.
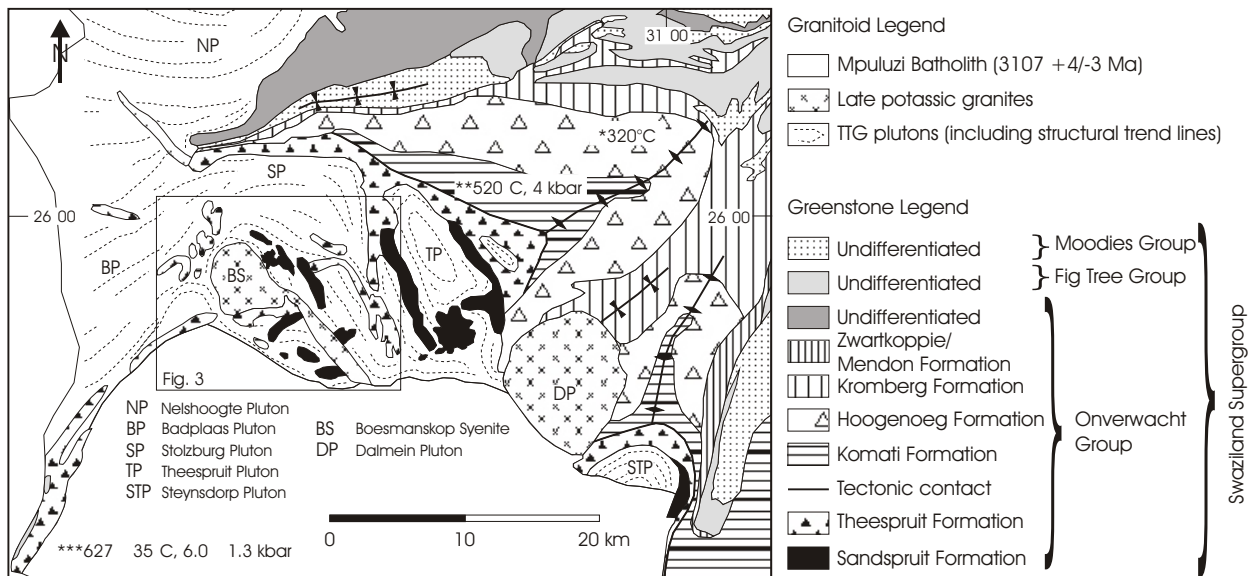
Figure 2: *Geological map and stratigraphic column of the southern part of the Barberton greenstone belt and the granite-greenstoneterrane to the south (modified after Anhaeusser et al., 1983, and Kröner et al., 1996). The estimated PT conditions for the peak metamorphic mineral assemblages from NE to SW are from *Xie et al. (1997), **Cloete (1991) and ***Stevens et al. (in prep.).*

A good understanding of the metamorphic history preserved in the rocks of the greenstone belt is essential to more fully understand the evolution of this remnant of Archaean crust. The purpose of this study is thus to reconstruct the metamorphic evolution of the greenstone remnants in the granite-greenstone terrane south of the greenstone belt. These rocks are located between two areas for which strikingly different metamorphic histories have been proposed (Fig. 2, Cloete, 1991, 1999; Stevens et al., in prep.). The investigation focuses on a sedimentary unit, which, at least in part, has been derived from reworking of older crustal material. For metamorphic purposes, these rocks are found to be the most useful in the area investigated.

GEOLOGY OF THE STUDY AREA

The granite-greenstone terrane to the southwest of the Barberton greenstone belt (Fig. 2) was first mapped and described by Anhaeusser (1980, 1983), Anhaeusser and Robb (1980) and Robb (1983b). Apart from the occurrence of numerous greenstone remnants in this area, these authors noted the polyphase nature of the adjacent trondhjemitic and tonalitic gneisses and the complex interaction of the granitoids and the greenstones commonly resulting in migmatization along their contacts. The contact relationships between the gneisses and greenstones were shown to be mostly intrusive, but mafic material intrusive into pre-existing trondhjemitic gneisses also exists. Kisters and Anhaeusser (1995b) attributed the concordant and discordant contact relationships between the Stolzburg and Theespruit plutons and the southern margin of the greenstone belt to a variety of simultaneously operating emplacement mechanisms, such as wall-rock deformation, stoping, assimilation and the intrusion of ring dykes. Lithologically, the greenstone remnants can be correlated with the lowermost formations of the Onverwacht Group (e.g., Viljoen and Viljoen, 1969; Anhaeusser, 1980). The remnants consist predominantly of mafic and ultramafic schists, interlayered banded iron formation and chert, and locally developed felsic agglomerates and tuffs as well as a metasedimentary unit formerly mapped as calc-silicate rocks. The strong layer-parallel foliation in most greenstone remnants is subvertical and can usually be traced into the adjacent trondhjemitic gneisses. The intense deformation and migmatization and the intrusion of syn- to late-tectonic felsic magmas has obscured the primary contact relationships in many places. However, the trondhjemites and tonalites that crosscut the original layering in several greenstone remnants, as well as numerous greenstone xenoliths within them, indicate a primary intrusive relationship (e.g., Robb, 1983b).
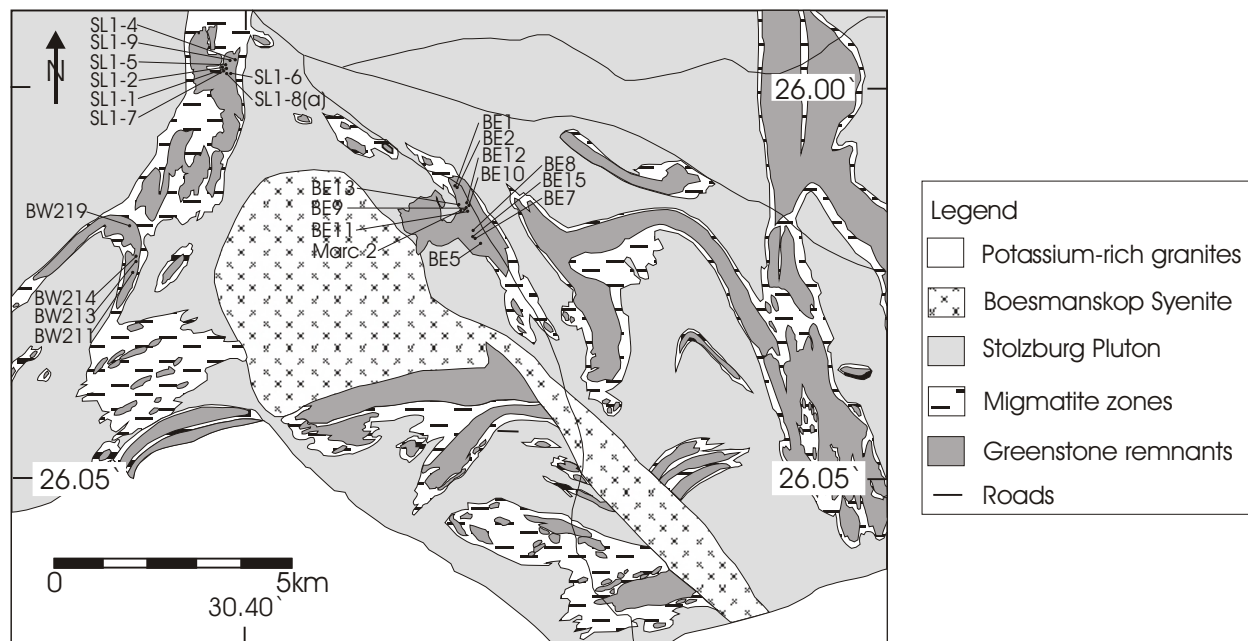
Figure 3*: Generalized geological map of the granite-greenstone terrane to the south of the Barberton greenstone belt, modified after Anhaeusser and Robb (1980), and including sample localities. Migmatite zones commonly occur along the contacts between the trondhjemitic-tonalitic gneisses and the greenstone remnants.*

The greenstone remnants investigated in this study (Fig. 3) are situated to the east and west of the *c*. 3107 Ma Boesmanskop syeno-granite complex (Anhaeusser et al., 1983; Kamo and Davis, 1994). Amphibolites (> 50%) are the dominant rock types, the remainder being ultramafic schists (serpentinites), banded iron formation and a clastic metasedimentary unit. The clastic

metasediments form a distinct, but minor component of all the greenstone remnants investigated in this study. These layers occur as discontinuous bands parallel to the main foliation and vary in thickness from 0.5 to 8m. Although their primary mineralogy has been replaced by metamorphic assemblages, original sedimentary features are locally preserved. Two texturally and mineralogically different varieties can be distinguished: the most common type is a fine-grained, compositionally banded and frequently boudinaged rock (Fig. 4), within which the chemical banding can be seen to be parallel to bedding planes in low strain domains. The second variety is medium- to coarse-grained and has a light pinkish colour. This variety is a potassium feldspar-rich impure arkose, characterised by well-defined bedding planes, and locally, by trough cross-beds (Fig. 4). The compositions of the metasediments (Table 1) reflect their heterogeneous nature. The highest K_2O concentrations in Table 1 correspond to the arkosic portions of the metasediments, whereas the high CaO and MgO concentrations occur in planar-bedded, compositionally banded portions. The loss on ignition (LOI) values are generally small, reflecting the relatively anhydrous mineralogy of the rocks and the absence of carbonate phases.
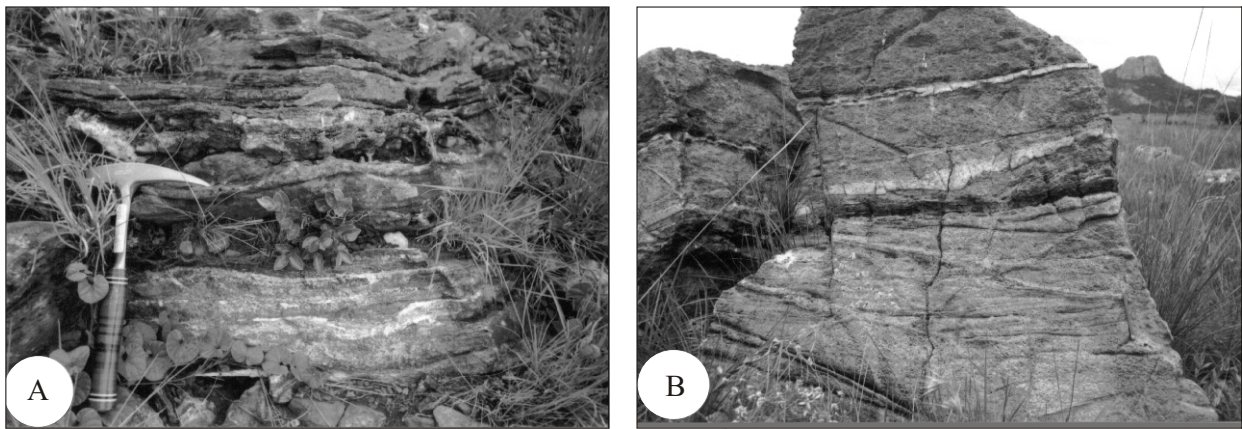
Figure 4: *(A) Finely banded and boudinaged metasediments from greenstone remnant SL1. (B) Boulder of a relatively undeformed, ungraded and cross-bedded arkose from greenstone remnant BE.*

GEOCHRONOLOGY

In order to constrain the age of the greenstone remnants both the arkosic portions of the metasediments (sample BE 5, Fig. 3) and a trondhjemite intrusive into the greenstone remnant BE sediments (sample Marc 2, Fig. 3) were sampled for zircon geochronology.

Analytical Techniques

Mineral separates were prepared from 4-6kg rock samples at the Hugh Allsopp Laboratory, University of the Witwatersrand, Johannesburg. Rock samples were pulverized using a heavy-duty hydraulic rock splitter, jaw crusher and swing mill. Mineral separation involved the use of a Wilfley table, heavy liquids (bromoform and methylene iodide) and a Frantz isodynamic separator.

U-Th-Pb SHRIMP analyses

Analyses were performed at the Research School for Earth Sciences (RSES) at the Australian National University, Canberra. Zircons were handpicked, mounted in epoxy resin and polished. Transmitted and reflected light microscopy, as well as SEM cathodoluminescence imagery was used to determine the internal structures of the zircons prior to analysis. Data were collected and

reduced as described by Williams and Claesson (1987) and Compston et al. (1992). U/Pb ratios were referenced to the RSES standard zircon AS3 standard (1099.1Ma, $^{206*}Pb/^{238}U$=0.1859, Paces and Miller, 1993). U and Th concentrations were determined relative to those measured in the RSES zircon standard SL13. All errors quoted in Table 2 are listed at 1, but where data are combined for regression analysis or to calculate weighted means, the final result is quoted with 95% confidence limits. All the geochronological statistical assessments were performed using the Isoplot/Ex program of Ludwig (2000).

Table 1: Whole rock major and trace element composition of the metasediments from 3 of the greenstone remnants investigated in this study

| Number | 1 | 2 | 3 | 4 | 5 | 6 | 7 | 8 | 9 | 10 | 11 | 12 | 13 | 14 | 15 | 16 |
Sample	SL1-6	SL1-8	SL1-8a	SL1-9	BE1	BE4*	BE5*	BE8	BE9	BE10*	BE11	BE12	BE13	BW211	BW214	BW219
SiO_2	64.06	55.87	71.02	55.77	57.51	81.25	62.7	55.88	53.7	85.43	77.19	61.62	54.6	54.02	51.54	69.29
TiO_2	0.26	0.54	0.3	0.29	0.82	0.2	0.22	0.46	0.47	0.24	0.22	0.74	0.85	0.53	0.9	0.26
Al_2O_3	9.4	4.86	10.57	10.89	11.9	6.23	11.96	6.33	7.35	7.69	5.68	13.93	12.51	13.03	17.05	11.4
Fe_2O_3	6.09	9.48	4.21	7.57	5.67	0.98	3.23	5.36	5.59	0.77	2.62	7.66	7.6	7.92	7.02	5.4
MnO	0.25	0.24	0.15	0.17	0.41	0.14	0.53	0.72	0.7	0.05	0.31	0.29	0.32	0.26	0.16	0.16
MgO	3.72	8.96	1.99	8.15	7.38	0.86	5.73	10.78	10.72	0.3	4.02	3.39	5.24	5.03	4.1	1.39
CaO	11.49	17.6	9.84	11.24	10.7	2.13	10.81	18.92	18.02	1.07	7.32	5	14.72	16.66	12.02	11.34
Na_2O	3.46	1.66	2.18	2.72	3.55	1.85	0.91	1.18	2.72	0.57	1.31	1.57	3.08	1.65	4.9	0
K_2O	0.55	0.49	0.24	1.34	1.21	3.41	3.75	0.2	0.4	4.23	1.04	4.3	0.65	0.15	0.46	0
P2O5	0.07	0.02	0.04	0	0.04	0.07	0.02	0.02	0.02	0.08	0.04	0.07	0.07	0.05	0.06	0.08
LOI	1.04	0.78	0.04	1.4	1.15	3.01	0.44	0.5	0.9	0.62	0.67	1.75	0.92	1.19	1.99	1.23
Total	100.39	100.5	100.49	99.56	100.34	100.13	100.31	100.35	100.59	101.05	100.43	100.33	100.56	100.49	100.22	100.57
Rb	34	44	22	63	79	104	59	29	35	64	89	124	41	21	20	8
Sr	331	147	206	232	346	181	63	129	222	32	113	68	333	166	224	169
Y	10	10	7	11	31	10	5	14	20	3	7	15	23	14	19	8
Zr	28	36	35	28	76	64	62	40	43	72	19	47	77	28	37	15
Nb	7	10	8	9	9	8	9	8	8	8	7	7	10	5	7	7
Co	48	65	34	51	74	11	9	39	50	9	22	48	57	43	57	27
Ni	464	372	307	420	560	26	9	295	418	11	187	156	295	165	217	163
Cu	2	2	2	2	2	9	2	2	2	2	9	97	38	12	941	40
Zn	56	86	56	64	140	705	28	104	99	31	51	97	91	57	1296	35
V	109	197	116	118	274	20	15	142	149	21	62	330	304	237	264	152
Cr	1729	1373	1559	1802	3356	30	23	1742	2007	26	677	160	1662	518	662	719
Ba	122	110	66	160	186	1829	1057	53	72	824	157	103	201	127	30	15

The analyses were conducted by standard X-ray fluorescence techniques utilizing the facilities in the Department of Geology, University of the Witwatersrand, Johannesburg. The analytical precision is better than 3% for major elements and about 5 to 10% For trace elements. * indicates arkosic samples

U-Pb conventional single zircon technique

Analyses were performed at the Hugh Allsopp Laboratory, University of the Witwatersrand. Zircons were examined using a binocular microscope and a scanning electron microscope in order to assess grain quality, degree of fracturing and the possible existence of inherited cores. Hand-picked zircons were abraded using the techniques of Krogh (1982) and washed in ultra-pure acetone and diluted nitric acid. Single zircon grains were then placed into 0.35 ml Teflon vials together with 30 l HF and a mixed ^{205}Pb-^{235}U spike. Eight of these Teflon vials were then placed in a Parr Container for 2 days at 220°C. The samples were chemically processed without separating U and Pb (Lancelot et al., 1976) and loaded on a rhenium filament together with a 0.25N phosphoric acid - silica-gel mixture. The analyses were performed on an automated VG54E mass spectrometer using a Daly collector and corrected by 0.12%/AMU for thermal mass fractionation. Total Pb blanks over the period of the analyses range from 15 to 30 pg and a value of 30pg was assigned as the laboratory blank ($^{206}Pb/^{204}Pb$=18.97 ± 1, $^{207}Pb/^{204}Pb$=15.73 ± 0.5 and $^{208}Pb/^{204}Pb$=39.19 ± 1.5). The calculation of common Pb was made by subtracting blanks and then assuming that the remaining common Pb has been incorporated into the crystal and has a composition determined from the

model of Stacey and Kramers (1975). Data were reduced using PbDat (Ludwig, 1993). Analytical uncertainties in Table 3 are listed at 2 and age determinations were processed using Isoplot/Ex (Ludwig, 2000).

Results

The arkose sample Be 5 contains relatively large zircons varying between 114-330 m in length. The predominant zircon type is dark purple in colour, needle-like in shape and has lengths varying from 210 to 330 m. Most grains are characterised by subrounded morphologies and surface textures consistent with mechanical transport and abrasion. A second abundant type, also purple in colour, is characterised by a smaller grain size and an oval shape, with a maximum length of about 190 m. These grains are generally more strongly rounded than the needle-shaped zircons (Fig. 5). As a consequence, their euhedral shape is not always preserved. A minor zircon type has a yellow to yellowish-brown colour and is oval-shaped. Cathodoluminescence imaging shows that all zircon types are usually concentrically and compositionally zoned. They are also characterised by different degrees of fracturing, mineral inclusions, such as apatite and feldspar, and a thin, uranium-poor overgrowth at their rims, which is interpreted to be metamorphic in origin.
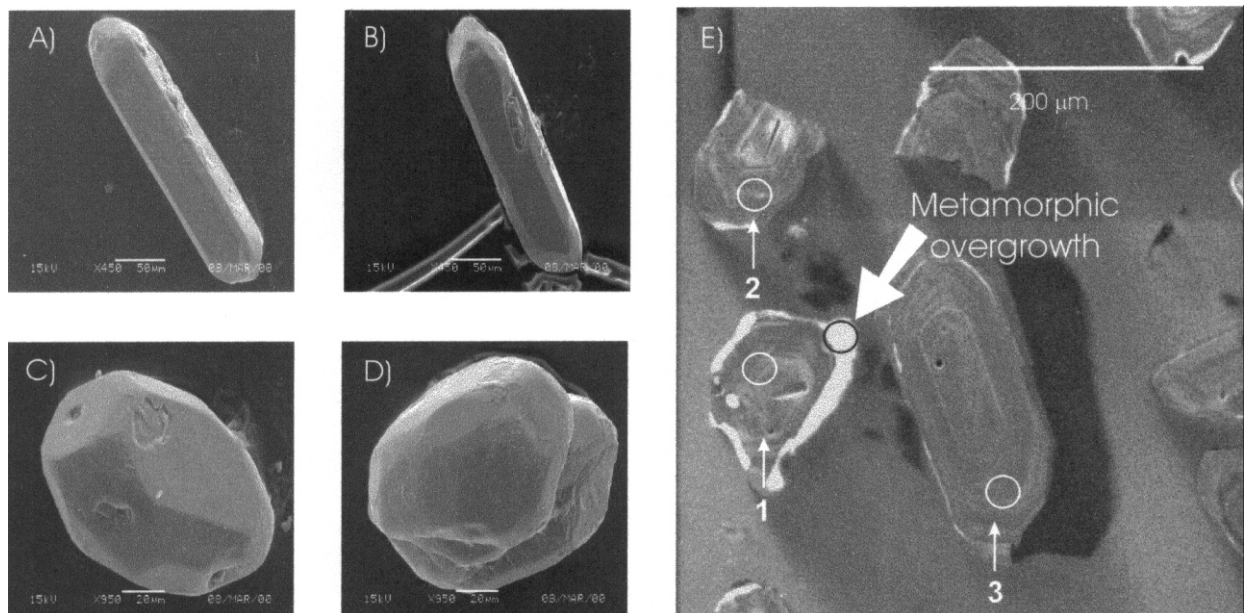
Figure 5: *SEM backscattered and cathodoluminescence images showing zircon morphologies and internal zonations in sample BE 5. (A, B) Euhedral, needle-shaped zircon grains with subrounded terminations. (C, D) Strongly rounded, oval-shaped zircon grains. (E) Concentrically zoned grains 1-3 (Table 2). Grain 1 shows a distinct bright metamorphic overgrowth.*

The results of 14 single grains analysed with the conventional technique (Table 3) and 26 spots from 25 different zircons analysed on SHRIMP I (Table 2) are plotted in Figure 6. Only isotopic ratios that are less than 10% discordant are considered as reliable indicators of age (inset in Fig. 6). All the data obtained from the conventional technique are more than 10% discordant and consequently will not be considered for further discussion. It is noteworthy that 14 of the 26 data sets obtained with the SHRIMP are also more than 10% discordant. As analyses of individual detrital grains record age information about the zircon-bearing source rocks, the ages of these grains are discussed in terms of their $^{207}Pb/^{206}Pb$ ages, which provide minimum age estimates of the rocks furnishing the grain. Excessive (>30%) degrees of discordance have been recorded for zircons from the Barberton greenstone belt (Tegtmeyer and Kröner, 1987). It appears likely, therefore, that some of the discordant detrital grains might have been discordant prior to their introduction into the arkose. It

Figure 6*: U-Pb concordia diagram summarizing the results of both conventional single zircon and SHRIMP dating techniques for the Barberton arkose (sample BE5). Inset shows data that are 90% concordant or more.*

is, however, also acknowledged that some of the discordance may have been superimposed during the post-depositional history of this unit. As mentioned previously, many of the grains investigated by cathodoluminescence imagery are characterised by bright, U-poor metamorphic overgrowths. Unfortunately, most of these rim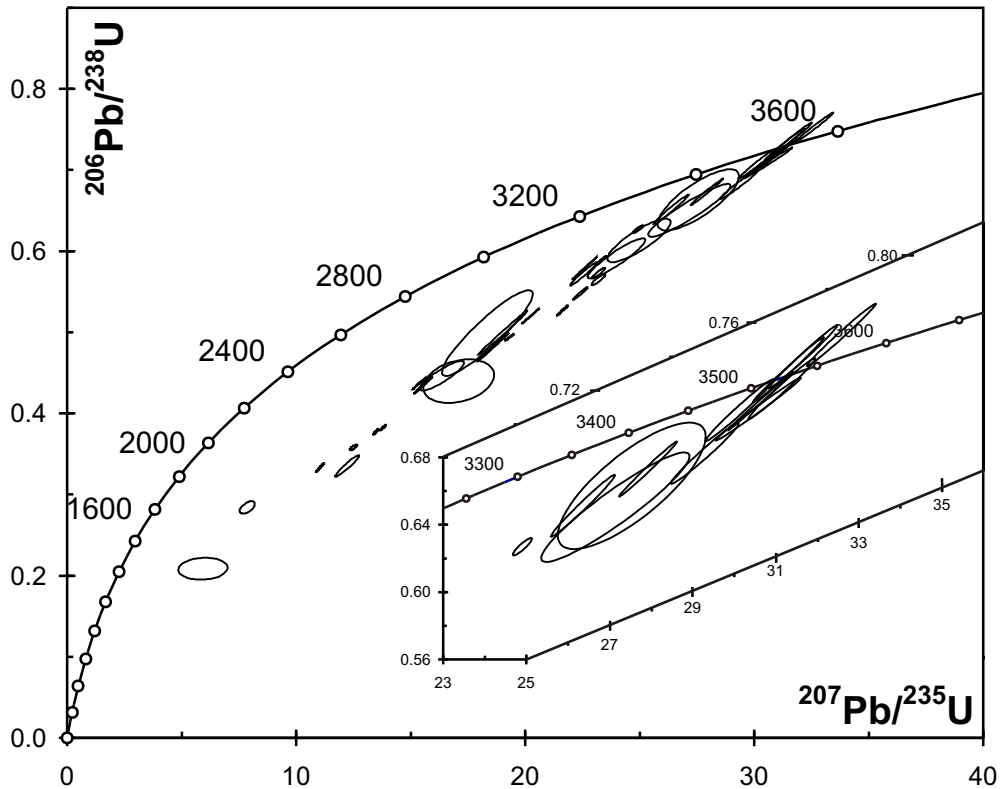s were too narrow to be analysed. One analysis, however (spot 1.2, Table 2, Fig. 5), provided a discordant (44%) ^{207}Pb/^{206}Pb age of 3293 ± 12 Ma while the rest of the grain gives a ^{207}Pb/^{206}Pb age of 3531 ± 6 Ma. Although this age could be regarded as the minimum age for the metamorphism, the *c.* 3230 Ma age on a syntectonic intrusion at Schapenburg (Stevens et al., in prep.), as well as age estimates on metamorphic sphenes from the Stolzburg pluton, which range between *c.* 3201 and 3255 Ma (Kamo and Davis, 1994), favour a younger event. Therefore, the age of *c.* 3293 Ma is interpreted as a "mixed" age.

A cumulative probability curve of the ^{207}Pb/^{206}Pb ages for data that are 90% concordant or more is shown in Figure 7. Four different peaks are recorded at 3442 Ma (1 zircon), 3479 Ma (3 zircons), 3526 Ma (4 zircons) and 3536 Ma (4 zircons). The Th/U ratios for these zircons vary between 0.13-0.78, but do not record any systematic trend with increasing (or decreasing) age. Similarly, the different mineral shapes described above do not correlate with any particular ^{207}Pb/^{206}Pb age. The oldest age of 3536 Ma is, within error, identical to an upper intercept age of 3538 6 Ma and 3538 +4 / -2 Ma reported by Armstrong et al. (1990) and Kamo and Davis (1994) for a wedge of tonalite gneiss located in the Theespruit Formation about 2 km northwest of the Doornhoek pluton (Fig. 1). The same age was also reported from an "older" zircon population in a volcaniclastic unit sampled 2m above the gneiss wedge (Armstrong et al., 1990). A granite boulder from Moodies Group conglomerates, dated at 3518 11 Ma by Kröner and Compston (1988), could also be related to the second peak at 3526 Ma. Another possible source terrane for the older set of zircons may be present in the southeastern part of the Barberton Mountain Land where Kröner et al. (1996) reported ages of

3502-3511 Ma for the Steynsdorp TTG pluton. This pluton yielded zircon xenocrysts as old as 3553 ± 4 Ma.

The peak at 3479 Ma could be correlated with an age found for a quartz-feldspar porphyry dyke intruding the Komati Formation (3470 +39 /-6 Ma, Kamo and Davis, 1994), as well as an age of a "magmatic" zircon population from a metagabbro intruding the Komati Formation (3482 5 Ma, Armstrong et al., 1990). The 3442 Ma peak (defined by only one grain) in Figure 7, although not well constrained, gives a maximum age for the deposition of the arkoses. It is, within error, identical to the intrusive age of the Stolzburg and other plutons at the southern margin of the greenstone belt (e.g., 3445 4 Ma, Kamo and Davis, 1994; see also below).
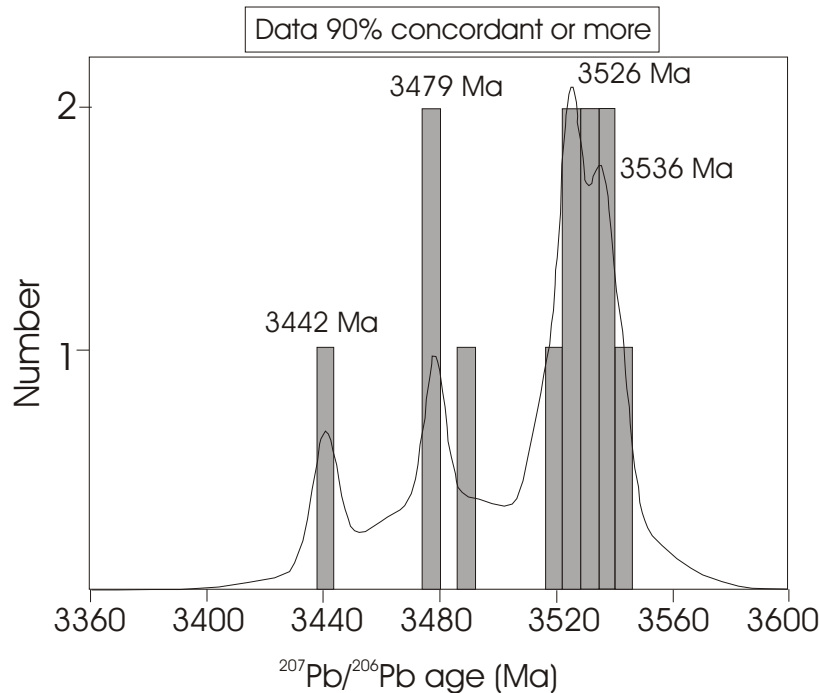
Figure 7: *Cumulative frequency distribution of $^{207}Pb/^{206}Pb$ ages of zircons from sample BE5 (12 analyses) - from analyses which are 90% or more concordant. Three distinct "peaks" occur at 3479, 3526 and 3536 Ma; a less well-constraind age is at 3442 Ma.*

Zircons extracted from a homogeneously foliated trondhjemite gneiss intrusive into the greenstone remnant BE and supposedly part of the Stolzburg pluton (Fig. 3) were analysed by the U-Pb conventional single-zircon technique. The Stolzburg trondhjemite is commonly characterised by the occurrence of two magmatic phases as a younger, fine-grained phase frequently crosscuts the pervasive fabric of the older trondhjemitic phase. The sample investigated in this study belongs to the older phase. The most abundant zircon type has a purple to yellowish-brown colour, a needle-like shape, and with grain sizes very similar to the zircons described above. Cathodoluminescence imaging of the zircons shows that they are all concentrically and compositionally zoned with the presence of prominent intra- and over-growths, the latter characterised by a bright colour in the CL images. Consequently, it would have proved difficult to select the best grains for dating by simple handpicking under a binocular microscope. Selected grains were, therefore, abraded following the technique described by Krogh (1982) and then mounted in epoxy for SEM imaging (Poller et al., 1997).

Table2: SHRIMP U-Th-Pb data for sample BE 5

Grain. spot	U (ppm)	Th (ppm)	Th/U	Pb* (ppm)	204Pb/ 206Pb	f206 %	206Pb/ 238U	±	207Pb/ 235U	±	207Pb/ 206Pb	±	206Pb/ 23	±	207Pb/ 235U	±	207Pb/ 206Pb	±	Conc. %
							Radiogenic Ratios						Apparent Ages (in Ma)						
1.1	148	73.8	0.5	131	0.000058	0.067	0.7131	0.0114	30.6800	0.5209	0.3120	0.0013	3470	43	3509	17	3531	6	98.3
1.2	106	10.5	0.1	39	0.000453	0.531	0.3335	0.0087	12.3100	0.3455	0.2677	0.0021	1856	42	2628	27	3293	12	56.4
2.1	215	84.2	0.39	185	0.000010	0.012	0.7077	0.0122	30.1610	0.5387	0.3091	0.0009	3450	46	3492	18	3516	5	98.1
3.1	517	189	0.37	303	0.000215	0.253	0.4984	0.0179	19.0950	0.6981	0.2779	0.0010	2607	78	3047	36	3351	5	77.8
4.1	389	88.7	0.23	277	0.000071	0.083	0.6122	0.0178	24.9850	0.9082	0.2960	0.0055	3079	72	3308	36	3449	29	89.3
5.1	277	148	0.53	256	0.000043	0.050	0.7395	0.0125	31.6910	0.5486	0.3108	0.0007	3569	46	3541	17	3525	4	101
6.1	499	230	0.46	265	0.000486	0.571	0.4455	0.0121	16.4380	0.6359	0.2676	0.0065	2375	54	2903	38	3292	39	72.2
7.1	569	228	0.4	393	0.000020	0.023	0.5786	0.0090	22.6310	0.3617	0.2837	0.0006	2943	37	3211	16	3384	3	87
8.1	404	316	0.78	353	0.000069	0.081	0.6727	0.0107	27.9680	0.4581	0.3015	0.0007	3316	41	3418	16	3478	4	95.3
9.1	236	176	0.75	232	0.000030	0.035	0.7526	0.0123	32.6110	0.5470	0.3143	0.0007	3617	45	3569	17	3542	4	102
10.1	252	33.7	0.13	214	0.000007	0.009	0.7319	0.0128	31.3480	0.5611	0.3107	0.0006	3540	48	3530	18	3524	3	101
11.1	548	150	0.27	314	0.000568	0.667	0.4982	0.0349	18.4020	1.3073	0.2679	0.0015	2606	152	3011	71	3294	9	79.1
12.1	240	78.2	0.33	205	0.000034	0.040	0.7083	0.0124	30.6200	0.6785	0.3135	0.0036	3452	47	3507	22	3538	18	97.6
13.1	300	69.3	0.23	228	0.000139	0.163	0.6510	0.0121	26.4130	0.5067	0.2943	0.0008	3232	48	3362	19	3440	4	93.9
14.1	407	100	0.25	271	0.000014	0.016	0.5713	0.0094	22.5910	0.3921	0.2868	0.0011	2913	39	3210	17	3400	6	85.7
15.1	342	141	0.41	274	0.000122	0.143	0.6627	0.0249	27.5830	1.1753	0.3019	0.0048	3278	97	3404	43	3480	25	94.2
16.1	498	303	0.61	263	0.000179	0.210	0.4336	0.0070	15.6130	0.2648	0.2612	0.0009	2322	32	2853	16	3254	5	71.4
17.1	733	129	0.18	224	0.000320	0.376	0.2828	0.0051	7.9686	0.2091	0.2044	0.0035	1605	25	2228	24	2862	28	56.1
18.1	243	96.6	0.4	172	0.000072	0.085	0.5901	0.0163	24.0200	0.8118	0.2952	0.0049	2990	66	3269	33	3445	26	86.8
19.1	765	144	0.19	177	0.001518	1.782	0.2064	0.0093	6.0413	0.7101	0.2123	0.0219	1210	50	1982	108	2923	178	41.4
20.1	627	211	0.34	400	0.000022	0.026	0.5519	0.2685	20.9180	10.2200	0.2749	0.0040	2833	1225	3135	638	3334	23	85
21.1	354	196	0.55	320	0.000049	0.058	0.7212	0.0119	31.1270	0.5258	0.3130	0.0006	3501	45	3523	17	3536	3	99
22.1	256	151	0.59	220	0.000177	0.208	0.6819	0.0120	29.3410	0.5360	0.3121	0.0010	3352	46.2	3465	18	3531	5	94.9
23.1	741	303	0.41	390	0.000010	0.012	0.4383	0.0177	17.1780	1.0163	0.2842	0.0110	2343	80	2945	58	3386	61	69.2
24.1	215	91.6	0.43	170	0.000082	0.097	0.6500	0.0215	27.1910	1.1707	0.3034	0.0072	3228	85	3390	43	3488	37	92.6
25.1	258	106	0.41	180	0.000041	0.048	0.5750	0.2490	23.5970	10.4380	0.2977	0.0153	2928	1109	3252	561	3458	82	84.7

* All errors are quoted at 1, but where data are combined for regression analysis or to calculate weighted means, the final result is Quoted with 95% confidence limits

Each of them was then photographed in both backscattered and cathodoluminescence SEM mode in order to   select inclusion- and intra- and/or over-growth-free grains. Six zircons were selected, removed from the epoxy mount and then processed (Table 3) following the procedure described above. Reported in a concordia diagram (Fig. 8), 5 grains define a discordia pointing to a well-defined upper intercept age of 3431 11 Ma (M.S.W.D. = 0.61) with a lower intercept age of 71 35 Ma. These results demonstrate the potential of selecting already abraded grains under cathodoluminescence control, adding a new parameter to the technique described by Poller et al. (1997). Although slightly younger, the age of 3431 ± 11Ma found for this sample is indistinguishable, within error, from the age of 3445 ± 4 Ma found for the Stolzburg pluton (Kamo and Davis, 1994, Fig. 1). Another explanation, however, may be that the age of *c*. 3431 Ma reflects a slightly younger pulse of magmatism in this area. Therefore, the sedimentation of the arkose is bracketed between 3442 and 3431 Ma, and must have occurred shortly before the intrusion of the Stolzburg pluton.

PETROGRAPHY

Fresh samples have been collected from the clastic metasediments, the amphibolite schists and the banded iron formation layers. The petrographical investigation of these rocks made use of more than 50 thin sections, most of which were from the highly heterogeneous clastic metasedimentary layers.

Amphibolites

The medium- to coarse-grained amphibolites have a well-developed schistosity in both hand sample and thin section. This fabric is mainly defined by the preferred orientation of elongated hornblende crystals. The investigated samples consist of green hornblende, quartz, plagioclase, clinopyroxene, actinolite, epidote, sphene and some opaque and semi-opaque material (probably
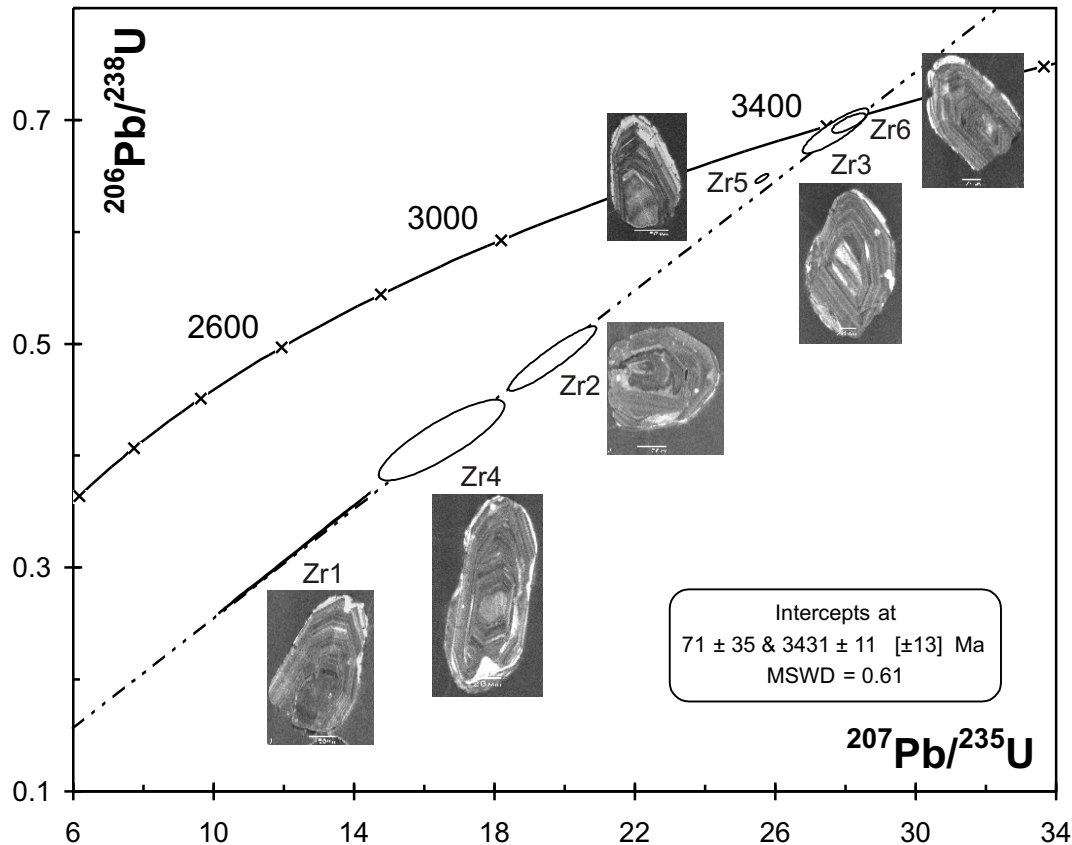
Figure 8: *U-Pb concordia diagram for a trondhjemite gneiss (Stolzburg pluton) showing the best fit regression line for the investigated zircons. Grain numbers correspond to those in Table 3.*

leucoxene) in decreasing order of abundance. The hornblende grains are characterised by sub-idiomorphic to xenomorphic crystal forms and vary in size between 100 m and 1 mm. They are light- to dark-green pleochroic and have thin actinolitic rims, which are colourless to light-green and only weakly pleochroic (Fig. 9a). Angular-to-rounded crystals of quartz and minor amounts of plagioclase form small aggregates at grain boundaries and triple-points between the hornblende crystals. Relic, sometimes poikilitic, clinopyroxene crystals of probable magmatic origin, with irregular grain forms and embayed grain boundaries, occupy only about 5 vol. % of the samples. They are about a few hundred m in diameter and are strongly altered to a fine-grained, brownish leucoxene along their rims and fractures. The leucoxene is sometimes intergrown with fine-grained hornblende and epidote. From textural evidence it is difficult to establish if the pyroxene was originally part of the peak metamorphic assemblage, but the fine-grained hornblende associated with the alteration products favours a magmatic origin for the pyroxenes.

Banded Iron Formation

The finely banded, oxide-facies iron formation forms narrow (up to half a metre thick) sedimentary horizons within the greenstone remnants. The common metamorphic mineral assemblage is quartz + magnetite + grunerite ± almandine ± orthopyroxene ± hornblende. The almandine garnets form large, rounded, crystals up to 3 mm in diameter and commonly contain quartz inclusions. Most of the garnet occurs within quartz-dominated layers, but it is locally associated with other phases such as orthopyroxene, grunerite and magnetite. The orthopyroxene crystals are 1 to 2 mm in diameter, strongly fractured, and often contain quartz inclusions. The grunerite occurs in two texturally different varieties (Fig. 9b). A peak-metamorphic generation of grunerite is colourless in thin section and characterised by well-developed multiple twinning. The poikiloblastic crystals, which are rich in inclusions of magnetite and quartz, have straight to slightly curved grain-boundaries and vary in size between a few hundred m and 2 mm. A retrograde generation of

grunerite replaces the orthopyroxe at crystal rims and along fractures. This fibrous grunerite forms a very fine-grained assemblage together with actinolite and magnetite (Fig. 9b). The garnet, however, does not show the same replacement textures. Hornblende occurs as rare inclusions in grunerite in sample SL1-5.

Table 3: U-Pb data for samples BE 5 and Marc 2

| Sample, Grain | Weight (µg) | U (ppm) | Pb (ppm) | Radiogenic Ratios | | | | | | | | Apparent age (in Ma) | | |
				$^{206}Pb/^{204}Pb$	$^{206}Pb/^{238}U$	±	$^{207}Pb/^{235}U$	±	$^{207}Pb/^{206}P$	±	$^{207}Pb/^{206}P$	$^{208}Pb/^{206}Pb$	Cor. Coef.
Be5													
Zr 1, b-p	10	325	141	1149	0.3757	0.6	13.550	0.6	0.2616	0.2	3256	0.062	0.96
Zr 2, b-p	9	281	105	959	0.3316	1.0	11.110	1.1	0.2430	0.2	3140	0.063	0.97
Zr 3, y-b, t	8	237	144	195	0.4339	1.2	15.302	1.2	0.2558	0.1	3221	0.099	0.99
Zr 4, p, t	5	119	53	169	0.3560	0.6	12.532	0.8	0.2553	0.4	3218	0.026	0.83
Zr 5, p	5	56	43	342	0.6263	0.5	24.966	0.6	0.2891	0.3	3413	0.075	0.91
Zr 6, d, p	9	322	210	675	0.5475	0.9	22.455	1.0	0.2975	0.2	3457	0.028	0.97
Zr 7, d, p	7	274	200	416	0.5719	0.7	23.238	0.8	0.2947	0.3	3442	0.085	0.92
Zr 2-1, p, t	7	206	119	1127	0.4803	2.4	18.673	2.4	0.2820	0.1	3374	0.093	1.00
Zr 2-2, y, t	8	186	83	1250	0.3809	0.6	13.856	0.6	0.2638	0.2	3270	0.095	0.96
Zr 2-3, p	6	226	137	1776	0.5192	1.3	20.285	1.3	0.2834	0.1	3382	0.074	1.00
Zr 2-4, p	6	334	233	2902	0.5886	0.6	23.379	0.6	0.2881	0.2	3407	0.088	0.96
Zr 2-5, p	7	121	77	1789	0.5257	0.7	21.649	0.8	0.2987	0.2	3463	0.098	0.98
Zr 2-6, t, d, p	8	153	104	1396	0.5639	0.8	23.250	0.9	0.2990	0.4	3465	0.088	0.90
Zr 2-8, p, t	9	210	121	5235	0.4932	0.6	19.353	0.6	0.2846	0.1	3388	0.073	0.98
Marc2													
Zr 1, p, t	6	197	79	348	0.3118	14.1	12.357	14.1	0.2874	0.2	3404	0.077	0.99
Zr 2, d, p, b	6	303	207	354	0.4859	4.8	19.697	5.2	0.2940	1.8	3439	0.149	0.93
Zr 3, p, t	5	80	53	294	0.6902	2.3	27.728	2.8	0.2914	1.3	3425	0.090	0.88
Zr 4, p, t	3	122	81	233	0.4128	7.0	16.550	8.8	0.2907	4.5	3422	0.299	0.86
Zr 5, p, t	6	113	77	294	0.6478	0.5	25.719	0.6	0.2879	0.2	3407	0.109	0.92
Zr 6, p, t	4	50	23	259	0.6972	1.0	28.102	1.4	0.2923	0.8	3430	0.177	0.78

*Errors are listed at 2 . Abbreviations: p = pink, b-p = brownish-pink, y-b = yellowish-brown, t = translucent, d = dark, y = yellow.

Clastic Metasediments

The clastic metasediments are macroscopically schistose rocks and are commonly characterised by a strong chemical banding. Sedimentary features, such as trough cross-bedding and bedding planes (Fig. 4) are only preserved in low-strain domains. They consist of quartzitic/arkosic layers alternating with green layers of a more mafic affinity, which will be referred to as mafic portions. Thin bands of amphibolite are also common within this unit. The metasediments show a wide range in their geochemical composition (Table 1). Compared to the adjacent amphibolites, the mafic portions are Si- and Ca-rich, but relatively Mg- and Fe-poor in bulk-composition and contain a variety of minerals including diopside, andesine, albite, garnet, quartz, epidote, sphene, microcline, and, locally, hornblende, chlorite, actinolite, leucoxene and sericite. Table 4 summarizes the main mineral assemblages in the samples investigated. Their inhomogeneous microtextures arecharacterised by the very local (cm- to mm-scale) development of equilibrium assemblages, abundant reaction textures, retrograde mineral zonation and possible prograde mineral inclusions in peak metamorphic minerals. These textures seem to be controlled by two factors: (1) the original mineralogy of the respective layers; and (2) the degree of retrograde replacement of peak metamorphic minerals. Due to major differences in the composition and mineral assemblages of these sediments within the study area, the typical textures in two greenstone remnants are described separately.

Greenstone remnant BE

Fine- to medium-grained arkosic layers, up to 10m thick, predominate in the clastic metasediments in greenstone remnant BE. The arkoses consist of microcline, quartz, plagioclase, diopside and minor amounts of epidote, actinolite, muscovite and chlorite. They also contain up to 4.3 wt% K_2O
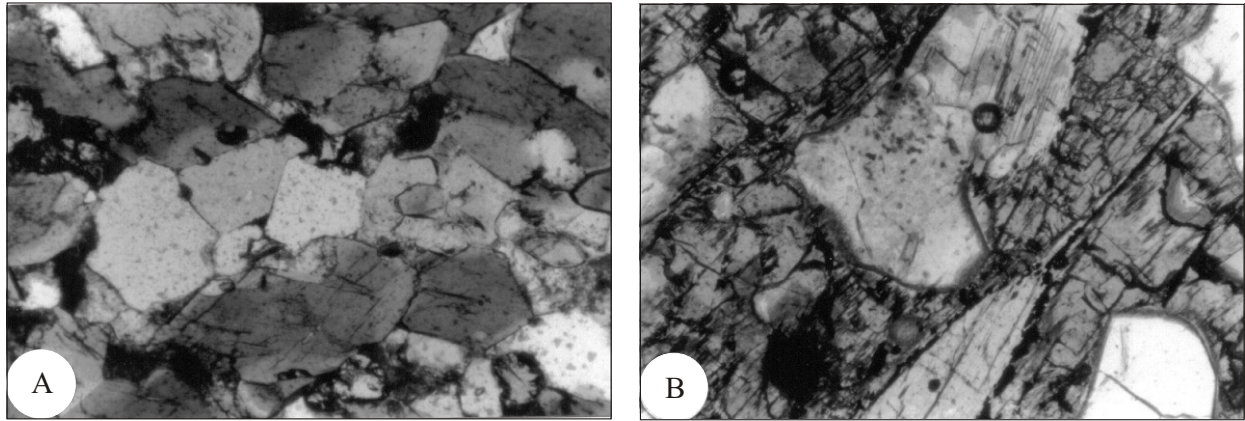

Figure 9: *Photomicrographs. (A) Peak metamorphic amphibole-quartz-plagioclase assemblage with relic clinopyroxene grains in sample BE 2. (B) Poikiloblastic orthopyroxene intergrown with wedge-shaped, peak metamorphic grunerite. Fine-grained aggregates of magnetite and a fibrous variety of grunerite and actinolite replacing orthopyroxene along rims and fractures and where in contact with peak metamorphic grunerite (Sample SL1-2).*

and are usually Ca-poor in bulk composition when compared to their mafic counterparts. The retrogression of the peak metamorphic minerals microcline, quartz, plagioclase, diopside and muscovite is minor and is marked by the replacement of muscovite by chlorite and the growth of fibrous actinolite needles and small epidote grains (~ 50 m) at triple points. The mafic portions are characterised by abundant coarse-grained and well-equilibrated clinopyroxene, which is indicated by straight grain-boundaries and 120 triple-points. Their texture varies on a mm-scale between granoblastic-polygonal and decussate. The size of the crystals ranges between 300 m and 1 mm. The clinopyroxene grains are colourless-to-greenish in thin-section. Although the shapes of the original xenomorphic plagioclase grains are still visible, most of them have been altered to a fine-grained assemblage of predominantly sericite, leucoxene, quartz, sphene and epidote. Coarse-grained crosshatched twins of microcline have occasionally grown within this fine-grained assemblage. More commonly, microcline is part of the peak metamorphic mineral assemblage and often forms a polygonal intergrowth with quartz, pyroxene, plagioclase and, occasionally, green hornblende within the mafic layers. Poikiloblastic garnets up to 2 mm in diameter are rare and have only been identified in one sample (BE 12). They contain inclusions of quartz, actinolite and altered plagioclase. Sample BE 12 is further characterised by the presence of chlorite and biotite, which have grown at the expense of muscovite. In general, retrogression in these rocks is localized and characterised by the replacement of pyroxene by medium-grained actinolite, and an occasionally extensive replacement of the peak metamorphic minerals by epidote and sphene (e.g., sample BE 13). The epidote crystals are generally round, are about 100 m in diameter and are pleochroic. The wedge-shaped sphene grains have grain sizes varying between 50 m and about 1 mm and, in places, occur in aggregates associated with epidote and leucoxene.

Greenstone remnant Sl1

The clastic metasediments in this greenstone remnant are up to 0.5m thick and form discontinuous

and commonly folded bands orientated parallel to the main foliation. Texturally, they are finely banded rocks in which feldspar-rich layers alternate with clinopyroxene-rich layers. The peak-metamorphic mineral assemblage for all samples is clinopyroxene + quartz + plagioclase + garnet + K-feldspar ± hornblende. The clinopyroxene grains are generally well preserved and commonly show a granoblastic polygonal texture. Their size ranges between about 200 m and 2 mm. They rarely have inclusions of possible prograde or peak metamorphic minerals such as amphibole, epidote, garnet and quartz. Most of the plagioclase has been extensively altered to sericite or to a fine-grained mixture of epidote, leucoxene, sphene and sericite (saussuritisation). Only samples SL1-9, SL1-8 and SL1-8a have relatively fresh plagioclase preserved. K-feldspar is usually associated with clinopyroxene and/or plagioclase. In contrast to sample locality BE it does not show the typical crosshatched microcline twinning. The garnet crystals vary between 500 m and 0.5cm in diameter. Epidote is one of the most common phases and replaces the garnet to different degrees grading from a partial replacement at the garnet rims to complete pseudomorphs after garnet (Fig. 10). Sample S11-9 and S11-1 do not contain any garnet and the minerals of the epidote group occur either as accessories (sample SL1-1) or not at all (sample SL1-9). In all other thin sections epidote is a major phase. Three types of epidote have been identified on the basis of textural relationships and different (interference) colours:

1.   A yellow pleochroic variety with second-order interference colours. It typically replaces garnet and more rarely clinopyroxene at its rims, or recrystallizes to irregular-shaped and fine-to medium-grained crystals with curved-to-embayed grain boundaries as an alteration product of plagioclase. This variety can be irregularly-to-concentrically zoned and sometimes forms pseudomorphs after garnet;

2.   A second variety of epidote is colourless-to-yellow in thin section with anomalous, light-blue interference colours. In sample S11-6 and SL1-8 it replaces a garnet crystal in its core, indicating a zonation in this garnet. More commonly, this epidote variety occurs in association with clinopyroxene and quartz and seems to form a stable, polygonal phase of the equilibrium assemblage; and

3.   A fine-grained epidote-variety occurs exclusively as a retrograde alteration product of plagioclase. This variety is iron poor and has a dark-bluish interference colour.

A common feature of all epidote is the development of a thin leucoxene rim, which does not exceed 200 m in thickness and appears brownish in thin section. This leucoxene appears to be a by-product

Table 4: Summary of the peak metamorphic mineral assemblages

Sample	Rock type	Peak metamorphic minerals	Retrograde phases	Mineral inclusions
BE1	Clastic Metased.	Hbl + Plg + Qtz + Cpx + (Spn)	Ser + (Ep)	Hbl + Qtz
BE2	Amphibolite	Hbl + Plg + Qtz	Ep + Ser + Act	Qtz
BE4	Clastic Metased.	Qtz + Cpx + Mc + Plg	Lcx + Act + Ep	------------
BE5	Clastic Metased.	Qtz + Plg + Mc + Ms + Cpx	Lcx + Ep	------------
BE7	Clastic Metased.	Qtz + Plg + Cpx + Ms	Lcx + Ser	Zrn
BE8	Clastic Metased.	Cpx + Qtz + Plg	Lcx + Ep + Spn	Qtz + Ep?
BE9	Clastic Metased.	Cpx + Plg+ Qtz + Mc	Mc + Act? + Ep + Spn + Lcx	Hbl + Qtz + Plg
BE10	Clastic Metased.	Qtz + Plg + Mc +Ms + (Ap)	Act + Ep	------------
BE11	Clastic Metased.	Qtz + Cpx + Mc + Hbl	Act	------------
BE12	Clastic Metased.	Qtz + Plg + Mc + Hbl + Grt	Chl + Bt + Spn + epidote + Lcx	------------
BE13	Clastic Metased.	Cpx + Plg + Qtz	Ep + Ser + Lcx	------------
BE15	Clastic Metased.	Qtz + Plg + Cpx	Ep + Ser	------------
BW211	Clastic Metased.	Hbl + Plg + Cpx + Qtz + Grt	Ep + Spn	Ep + Act + Hbl
BW213	Clastic Metased.	Hbl + Plg + Qtz	Ep + Spn	------------
BW214	Clastic Metased.	Hbl + Plg + Qtz	Ep + Lcx	------------
BW219	Clastic Metased.	Cpx + Qtz + Ep	Ep + Act	------------
SL1-1	Clastic Metased.	Cpx + Plg + Qtz	Ep + Spn + Act + Ser	------------
SL1-2	Iron Formation	Qtz + Mag + Gru + Opx + Grt	Gru + Act + Mag	------------
SL1-5	Iron Formation	Qtz + Mag + Gru + Opx + Hbl	Gru + Act + Mag	------------
SL1-6	Clastic Metased.	Cpx + Plg + Qtz + Grt + Mc	Ep + Act + Spn + Lcx + Ser	Hbl + Ep +Spn + Qtz + Plg
SL1-8	Clastic Metased.	Cpx + Qtz + Grt + Plg	Ep + Spn +Ser	Act
SL1-8a	Clastic Metased.	Cpx + Plg +Qtz + Grt + Hbl	Ep + Ser	Qtz + Hbl + Spn + Grt
SL1-9	Clastic Metased.	Cpx + Plg + Hbl + Qtz	Ser	Hbl

Mineral abbreviations are after Kretz (1983), except for Lcx (leucoxene) and Ser (sericite). Metased. = Metasediment

of the retrograde replacement of garnet by epidote. The sphenes are diamond-shaped and about 200-300 m in size. Most commonly, they occur together with the yellow-pleochroic variety of epidote where it replaces garnet, but are also associated with clinopyroxene, or have inclusions of clinopyroxene.

MINERAL CHEMISTRY

A detailed investigation of the mineral chemistry of the selected samples was carried out at the Rand Afrikaans University, Johannesburg. Samples were targeted for detailed study where metamorphic reaction textures, significant mineral inclusions and evidence for chemical zonation of minerals had been identified. Minerals were analysed for major elements using a Cameca 255-electron microprobe operating at 15 kV with a Link EXL2 energy-dispersive spectrometry system. The spectra were processed by ZAF corrections. The accuracy of the analyses varies from element to element, but is considered to be less than 1% of the measured value for most of the major elements. X-ray compositional maps were acquired using a Noran Vantage EDS with a digital pulse processor. The dwell time was 20 microseconds with a resolution of 1024 x 1024 pixels. Mineral abbreviations are after Kretz (1983).
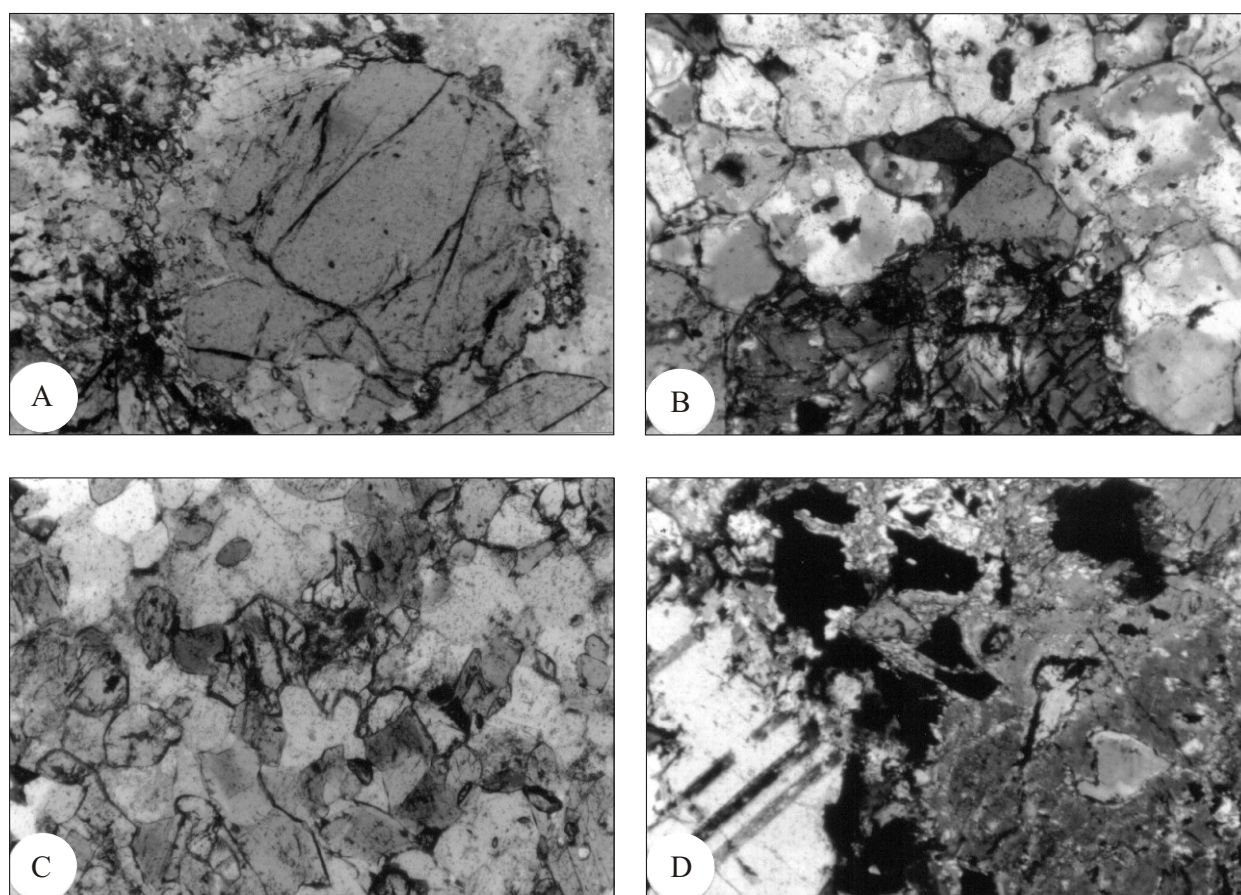
Figure 10: Photomicrographs illustrating mineral assemblages and typical replacement textures in the clastic metasediments. (A) Partial replacement of garnet by epidote of the first variety in sample SL1-6. The replacing epidote is recognized by the dark leucoxene rim surrounding it. The light-grey mineral in the background is albite; the mineral in the lower right corner is sphene. (B) Granoblastic-polygonal epidote grains of the second variety in contact with clinopyroxene in sample SL1-8. (C) Hbl-Plg-Cpx-Qtz assemblage in sample BE 1. (D) Partially replaced Cpx-Grt-Qtz-Plg assemblage in sample SL1-6.

Amphibolite (Sample BE 2)

According to the Leake et al. (1997) classification diagram for calcic amphiboles with ANa + AK < 0.5 and Ti < 0.5, the amphiboles in this sample are magnesio-hornblende with actinolite rim compositions (Fig. 11) (Table 5). The amphiboles are characterised by a Mg/(Mg + Fe^{2+}) ratio of 0.65-0.78, with the actinolitic rims having slightly higher ratios than the cores. The total Si concentration varies between 6.97-7.77 a.p.f.u. The plagioclase is andesine with XAb ranging between 0.52 and 0.54 (Table 5). Plagioclase grains contain only traces of potassium with values between 0.015 and 0.052 a.p.f.u. The composition of the clinopyroxene, interpreted to be a relic magmatic mineral, has been variably altered, as indicated by the low totals as well as the strongly variable Mg/(Mg+Fe) ratios (0.71-0.92, Table 5).
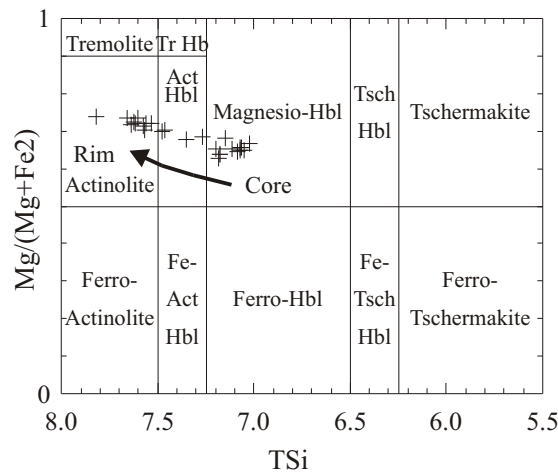
Figure 11: Classification diagram for calcic amphiboles from sample BE 2 after Leake et al. (1997). The zoned amphiboles have magnesio-hornblende cores and actinolite rims.

Banded Iron Formation (Samples SL1-2, SL1-5)

The garnet in this rock type is almandine with an average composition of Xalm = 0.74-0.79, Xgrss = 0.13-0.17, Xpyp = 0.04-0.07 and Xspss = 0.03-0.04 (Table 6). The Fe/(Fe+Mg)-ratio ranges between 0.92-0.95. The garnet does not record any marked compositional changes towards crystal rims, except for a slight increase in the Ca concentration (Table 6). Metamorphic orthopyroxene is slightly zoned from core to rim. The cores have Fe/(Fe+Mg) ratios between 0.81-0.82. In contact with grunerite the Fe-number decreases to 0.77-0.79 and the Ca-concentration decreases from ~0.029 a.p.f.u. to ~0.02 a.p.f.u. The grunerite appears unzoned and has almost identical Fe-numbers compared to the orthopyroxene, with values ranging from 0.77-0.81. Grunerite, in contact or intergrown with calcic amphibole, has generally lower Mg-concentrations and, therefore, higher Fe-numbers. The calcic amphiboles can be classified as ferro-hornblendes (Leake et al., 1997).

Clastic Metasediments (Samples SL1-6, SL1-8 and SL1-8a)

The garnet is Ca-rich and forms essentially grossular-almandine solid solutions. It does not record any marked compositional variation within the grains, but where epidote replaces garnet crystals at their rims and/or cores there is an increase of Ca, Mn and Cr, and a decrease of Fe and Mg. The Fe/(Fe+Mg) also increases towards the garnet rims (Figs. 12 and 13). Although all garnet grains show the same type of zonation, their composition differs in terms of their absolute Ca, Mn, Cr, Fe and Mg concentrations (Table 7 and Fig. 14). Those garnet cores that have not been replaced by epidote have an average composition of Xgrss = 0.59, Xalm = 0.32, Xpyp =

Table 5: Major element content and structural formulae for amphiboles (cations per 23 oxygen), plagioclases (cations per 32 oxygen), and clinopyroxenes (cations per 6 oxygen)

Sample	BE2	BE2	BE2	BE2	BE2	BE2	Sample	BE2	BE2	BE2	BE2	Sample	BE2	BE2	BE2	BE2
Mineral	Hbl	Hbl	Hbl	Hbl	Hbl	Hbl	Mineral	Plg	Plg	Plg	Plg	Mineral	Cpx	Cpx	Cpx	Cpx
Location	rim	core	core	rim	core	rim										
SiO_2	52.465	48.204	48.276	52.374	52.343	48.09	SiO_2	57.73	57.95	55.37	54.84	SiO_2	54.23	52.67	52.01	50.04
TiO_2	0.125	0.522	0.478	0.319	0.283	0.47	TiO_2	0	0	0.04	0	TiO_2	0.05	0.42	0.06	0.49
Al_2O_3	3.427	8.121	8.267	3.974	3.168	7.3	Al_2O_3	32.31	32.14	26.73	26.89	Al_2O_3	1.33	0.77	0.84	5.78
FeO	11.149	12.935	12.931	11.106	11.169	12.09	FeO	0.3	0.19	0.07	0.1	FeO	7.36	3.59	7.65	12.88
Cr_2O_3	0.224	0.287	0.18	0.442	0.079	0.24	Cr_2O_3	0	0	0	0	Cr_2O_3	0.04	0.02	0.23	0.34
MnO	0.181	0.205	0.279	0.294	0.307	0.29	MnO	0.02	0	0	0	MnO	0.26	0.06	0.33	0.17
MgO	15.849	13.485	13.639	15.529	15.782	13.55	MgO	0	0	0	0	MgO	12.3	16.48	13.24	14.37
CaO	12.542	11.892	12.335	12.514	12.588	12.2	CaO	10.01	9.98	9.39	9.16	CaO	21	25.06	23.29	12.42
Na_2O	0.324	0.708	0.885	0.377	0.206	0.46	Na_2O	6.22	6.53	5.53	5.52	Na_2O	0.43	0.29	0.24	0.41
K_2O	0.105	0.364	0.344	0.123	0.08	0.28	K_2O	0.11	0.07	0.22	0.07	K_2O	0.07	0	0	0.29
Total	96.391	96.723	97.614	97.052	96.005	94.97	Total	99.47	100.12	100.62	100.9	Total	97.07	99.36	97.89	97.19
TSi	7.617	7.073	7.023	7.573	7.625	7.152	Si	9.769	9.773	10.175	10.197	TSi	2.08	1.93	1.98	1.92
TAl	0.383	0.927	0.977	0.427	0.375	0.848	Al	6.39	6.359	5.838	5.821	TAl	0.00	0.03	0.02	0.08
CAl	0.203	0.477	0.439	0.25	0.169	0.431	Ti	0	0	0.006	0	TFe^{3+}	0.00	0.03	0.00	0.00
CCr	0.026	0.033	0.021	0.05	0.009	0.028	Fe^{2+}	0.042	0.027	0.011	0.016	M1Al	0.06	0.00	0.02	0.18
CFe^{3+}	0.016	0.032	0.099	0	0.061	0.098	Mn	0.003	0	0	0	M1Ti	0.00	0.01	0.00	0.01
CTi	0.014	0.058	0.052	0.035	0.031	0.053	Ca	1.799	1.803	1.842	1.838	$M1Fe^{3+}$	0.00	0.06	0.01	0.00
CMg	3.43	2.95	2.958	3.347	3.428	3.004	Na	2.023	2.135	1.988	2.005	$M1Fe^{2+}$	0.23	0.02	0.21	0.00
CFe^{2+}	1.311	1.451	1.431	1.318	1.299	1.386	K	0.024	0.015	0.052	0.017	M1Cr	0.00	0.00	0.01	0.01
CMn	0	0	0	0	0.003	0	Cations	20.05	20.11	19.91	19.95	M1Mg	0.71	0.90	0.75	0.79
BFe^{2+}	0.027	0.105	0.043	0.025	0	0.019	Xab	0.53	0.54	0.52	0.52	M2Mg	0.00	0.00	0.00	0.03
BMn	0.022	0.025	0.034	0.036	0.035	0.037	Xan	0.47	0.46	0.48	0.48	$M2Fe^{2+}$	0.01	0.00	0.02	0.41
BCa	1.951	1.87	1.923	1.939	1.965	1.944						M2Mn	0.01	0.00	0.01	0.01
ANa	0.091	0.201	0.25	0.106	0.058	0.133						M2Ca	0.87	0.99	0.95	0.51
AK	0.019	0.068	0.064	0.023	0.015	0.053						M2Na	0.03	0.02	0.02	0.03
Cations	15.11	15.27	15.31	15.13	15.07	15.18						M2K	0.00	0.00	0.00	0.01
XMg	0.72	0.65	0.67	0.71	0.73	0.68						Cations	4.00	4.00	4.00	3.99
												XMg	0.71	0.90	0.75	0.82

0.021 and Xspss = 0.06. For comparison, the garnet rim in Figure 12, which is in contact with retrograde albite and epidote, has an average composition of Xgrss = 0.647, Xalm = 0.252, Xpyp = 0.005 and Xspss = 0.095. Garnet grains that show extensive replacement at both core and rim are relatively depleted in Ca and enriched in Fe, and have an average composition of Xgrss = 0.56, Xalm = 0.35, Xpyp = 0.026 and Xspss = 0.064. The X-ray composition maps in Figure 13 show the relative distribution of selected elements in epidote and garnet. It should be noted that this garnet also has a thin retrograde rim along the contact with epidote in its core. Therefore, those garnet cores that did not re-equilibrate with epidote, e.g., garnets that have only been replaced by epidote at their rims give the best estimate for the peak metamorphic composition of garnet. The range in mineral compositions for clinopyroxene is relatively small. The Mg-numbers range from 0.55 to 0.66, two high values (0.70 and 0.72) coming from pyroxene in close proximity to epidote. The Ca-content ranges from 0.924 to 0.97 a.p.f.u. In the classification diagram of Morimoto (1988), all data fall within the field for diopside. The Fe^{3+} has been recalculated by charge balance (Table 8). The pyroxene does not show any zonation with respect to Al, except where it is comparatively Al-poor when partially replaced by epidote along its rims and fractures. The total Al range varies between 0.003 and 0.082, but most of the analyses scatter between 0.44 and 0.68.

Plagioclase appears unzoned, but the extensive alteration of many grains may mask the zonation, as it is impossible to measure traverses on single grains. However, plagioclase in contact with both the garnet rims and epidote is almost pure albite (Xan = 0.01-0.09, Table 9), whereas the plagioclase away from the garnet is andesine (Xan = 0.34-0.36, Table 9). The latter is usually associated with clinopyroxene, quartz and sometimes microcline. No plagioclase with an intermediate composition between andesine and albite has been identified, although one grain in sample SL1-8a records slightly lower Ca concentrations with a Xan of 0.30-0.32. Sample SL1-6, with a high abundance of garnet, contains only albite. The Ps (Fe^{3+}/Fe^{3+} + Al, Table 10) content of epidote ranges between 0.10-0.28. In general, epidote grains of the third variety are relatively poor in Fe, and have a Ps

Table 6: Major element content and structural formulae for garnets (cations per 24 oxygen), grunerite (cations per 23 oxygen) and orthopyroxene (cations per 6 oxygen)

Garnet:

Sample	SL1-2	SL1-2	SL1-2	SL1-2	SL1-2	SL1-2
Mineral	Grt	Grt	Grt	Grt	Grt	Grt
Location	core	core	core	rim	core	core
SiO_2	37.03	36.46	37.03	36.98	37.17	37.12
TiO_2	0.08	0.01	0	0	0	0.08
Al_2O_3	20.46	20	20.21	20.99	20.79	20.41
Cr_2O_3	0.04	0	0	0	0.08	0
FeO	35.44	35.57	35.02	33.89	34.82	35.48
MnO	1.74	1.56	1.74	1.63	1.43	1.53
MgO	1.07	1.23	1.56	1.23	1.25	1.18
CaO	4.9	5.02	5.33	5.92	5.25	5.28
Na_2O	0	0.08	0.22	0.09	0.16	0.14
K_2O	0	0	0.02	0	0	0
Cl_2O	0	0	0.02	0	0	0
ZrO_2	0	0	0.05	0	0	0
NiO	0	0.12	0	0	0.03	0.23
Total	100.77	100.05	101.19	100.72	100.97	101.46
TSi	6.022	6.052	6.076	6.002	6.028	6.048
TAl	0	0	0	0	0	0
AlVI	3..918	3..91	3..906	4.012	3..97	3.916
Fe^{3+}	0.4	0.85	2.948	3.256	3.376	3.992
Ti	0.01	0.002	0	0	0	0.01
Cr	0.006	0	0	0	0.01	0
Fe2	4.692	4.596	4.388	4.406	4.528	4.562
Mg	0.26	0.304	0.382	0.298	0.302	0.286
Mn	0.24	0.22	0.242	0.224	0.196	0.212
Ca	0.854	0.892	0.938	1.03	0.912	0.922
Na	0	0.026	0.07	0.028	0.05	0.044
XGrss	0.141	0.148	0.158	0.173	0.154	0.154
XAlm	0.776	0.764	0.737	0.74	0.763	0.763
XPyp	0.043	0.051	0.064	0.05	0.051	0.048
XSpss	0.04	0.03	0.03	0.02	0.02	0.02
Cations	16.4	16.85	18.94	19.25	19.37	19.99
XFe	0.95	0.94	0.95	0.96	0.96	0.96

Grunerite:

Sample	SI1-2	SI1-2	SI1-2	SI1-2	SI1-2
Mineral Type	Gru peak	Gru peak	Gru peak	Gru peak	Gru peak
SiO_2	48.96	48.8	48.67	49.24	49.2
TiO_2	0	0.14	0	0.03	0.03
Al_2O_3	0.27	0	0.39	0.41	0.36
FeO	39.15	39.36	39.31	39.96	39.78
Cr_2O_3	0.07	0	0.07	0.02	0
MnO	0.79	0.61	0.7	0.64	0.75
MgO	6.3	6.38	6.28	6.49	6.52
CaO	0.53	0.57	0.65	0.6	0.5
Na_2O	0.41	0.56	0.67	0.43	0.3
K_2O	0	0	0	0	0.01
Cl_2O	0.05	0	0	0.05	0.04
ZnO	0	0	0.18	0.44	0.18
NiO	0.17	0	0	0	0.32
Total	96.7	96.45	96.91	98.31	98.01
TSi	7.922	7.917	7.874	7.854	7.867
TAl	0.051	0	0.074	0.077	0.068
TFe^{3+}	0	0	0	0.069	0.065
TTi	0	0.017	0	0	0
CCr	0.009	0	0.009	0.003	0
CFe^{3+}	0	0	0	0.003	0.03
CTi	0	0	0	0.004	0.004
CMg	1.52	1.543	1.515	1.543	1.554
CFe^{2+}	3.471	3.457	3.476	3.447	3.412
BFe^{2+}	1.826	1.883	1.843	1.811	1.813
BMn	0.108	0.084	0.096	0.086	0.102
BCa	0.065	0.033	0.061	0.103	0.086
ACa	0.026	0.066	0.051	0	0
ANa	0.129	0.176	0.21	0.133	0.093
AK	0	0	0	0	0.002
Cations	15.12	15.17	15.21	15.13	15.09
XFe	0.78	0.78	0.78	0.78	0.77

Orthopyroxene:

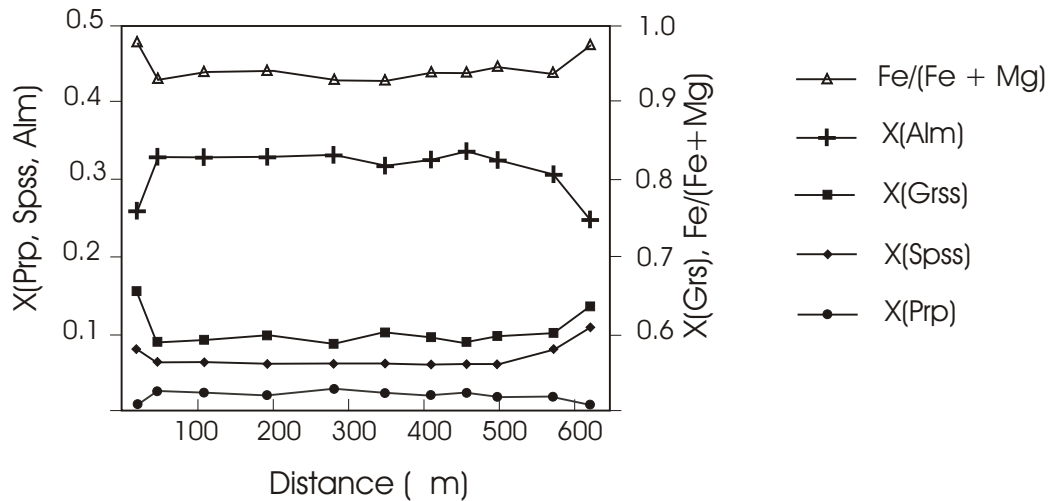| Sample	SL1-2	SL1-2	SL1-2	SI12	SL1-2
Mineral	Opx	Opx	Opx	Opx	Opx
Location	core	core	core	core	rim
SiO_2	46.73	46.81	46.65	46.55	50.83
TiO_2	0	0.01	0	0	0.08
Al_2O_3	0.15	0.24	0.2	0.14	0
FeO	45.8	44.96	45.01	44.57	40.17
Cr_2O_3	0	0	0.19	0	0
MnO	1.06	1.14	1.09	0.95	1.05
NiO	0	0	0.1	0.31	0.14
MgO	6.04	5.72	5.88	5.81	6.55
CaO	0.56	0.66	0.64	0.67	0.44
Na_2O	0.67	0.62	0.57	0.56	0.38
K_2O	0	0	0.01	0.01	0.04
Cl_2O	0.01	0	0	0	0.02
ZnO	0.08	0.07	0	0	0
Total	101.1	100.23	100.33	99.58	99.71
TSi	1.927	1.948	1.939	1.949	2.107
TAl	0.007	0.012	0.01	0.007	0
TFe^{3+}	0.066	0.04	0.052	0.044	0
M1Ti	0	0	0	0	0.002
$M1Fe^{3+}$	0.127	0.101	0.101	0.097	0
$M1Fe^{2+}$	0.502	0.544	0.525	0.53	0.588
M1Cr	0	0	0.006	0	0
M1Mg	0.371	0.355	0.364	0.363	0.405
M1Ni	0	0	0.003	0.01	0.005
$M2Fe^{2+}$	0.885	0.88	0.887	0.89	0.804
M2Mn	0.037	0.04	0.038	0.034	0.037
M2Ca	0.025	0.029	0.028	0.03	0.02
M2Na	0.054	0.05	0.046	0.045	0.031
M2K	0	0	0.001	0.001	0.002
Cations	4	4	3.99	3.99	3.99
XFe	0.81	0.81	0.81	0.81	0.77

Figure 12: Compositional variations in the partially replaced garnet grain shown in Figure 10A. The inner parts of this garnet grain are not zoned. Only a thin rim along the contacts with epidote and albite records increasing Ca, Mn and Cr concentrations and decreasing Fe and Mg concentrations.
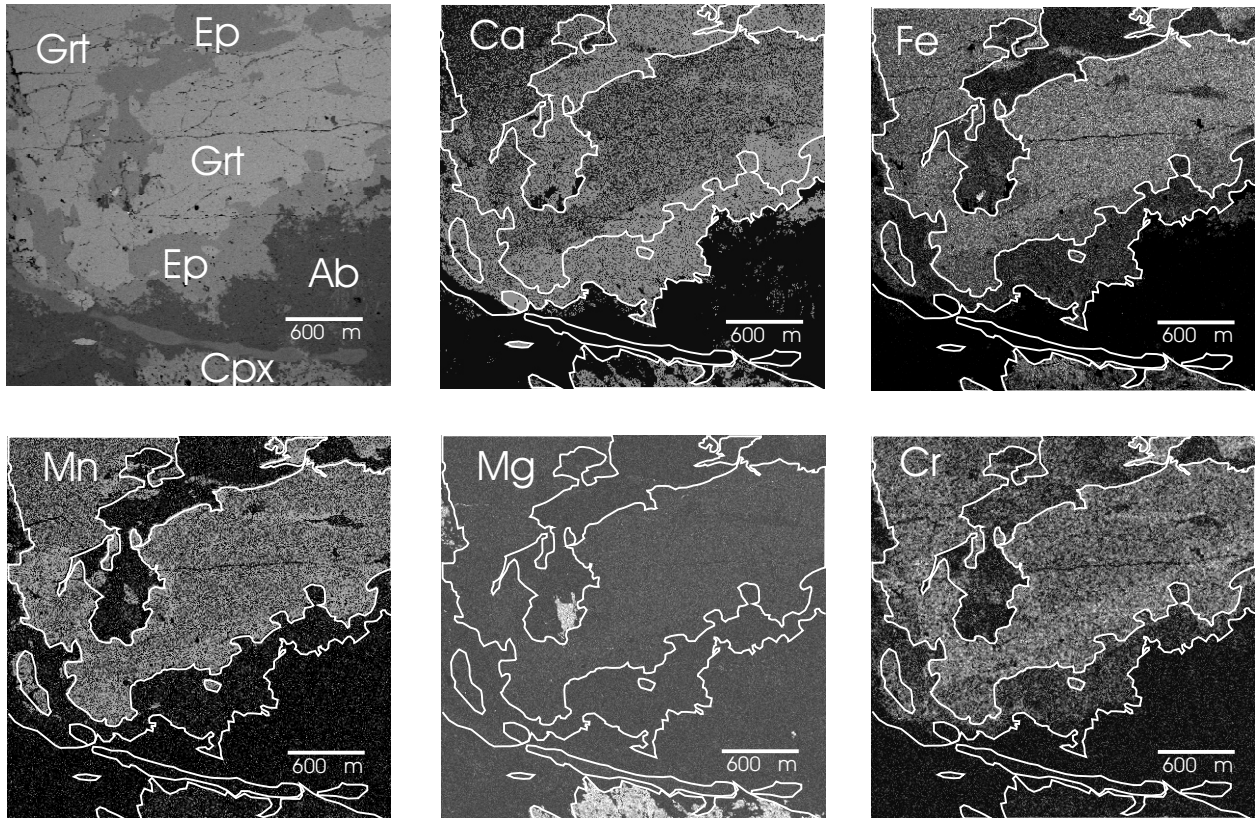
***Figure 13**: SEM image and X-ray composition maps for selected elements in garnet and epidote. Lighter colours correspond to increasing concentrations, darker colours mark areas with low concentrations of the respective elements.*
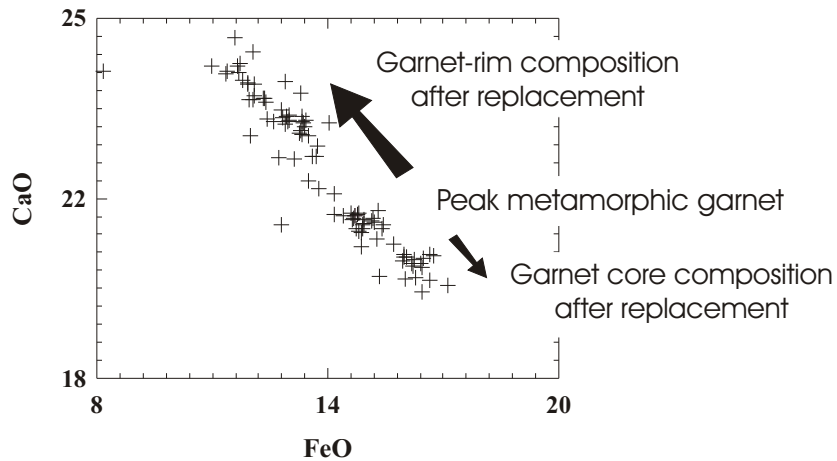

***Figure 14**: Ca-Fe variations in garnet, in response to the retrograde replacement of garnet by epidote. The 93 microprobe analyses, carried out on 5 different garnet grains, show either rim replacement or both core and rim replacement, except for sample SL1-8a, where a garnet inclusion in Cpx has been analysed.*

content of 0.11-0.13 pfu. However, their cores occasionally record Ps values of 0.20. Epidote grains of the second variety, that replace the garnet cores, are relatively enriched in Fe, with an average Ps content 0.17 pfu. The Ps content of epidote replacing garnets at their rims seems to depend on the degree of replacement. In assemblages where epidote only replaces the garnet rims, the Ps content is 0.18-0.23. Assemblages that show both core and rim replacement have Ps (rim) of 0.13-0.19. Those epidote grains that form pseudomorphs after garnets are irregularly to concentrically zoned, with Ps 0.11-0.18.

Table 7: Major element content and structural formulae of garnets (cations per 24 oxygen)

Sample	SL1-6	SL1-6	SL1-6	SL1-6	SL1-6	SL1-6	SL1-6	SL1-6	SL1-6	SL1-8	SL1-8	SL1-8	SL1-8a
Location	core	core	rim	rim	rim	core	rim	core	core	core	rim	core	*incl.
SiO_2	39.05	38.35	38.76	38.52	38.46	38.53	38.71	38.61	38.36	38.78	38.81	38.32	38.7
TiO_2	0.2	0.26	0.03	0.02	0	0.26	0.09	0.25	0.12	0.22	0.01	0.05	0.22
Al_2O_3	19.29	18.78	18.72	18.4	18.9	18.57	18.68	19.28	18.61	19	19.2	18.91	18.27
Cr_2O_3	2.93	3.19	3.11	3.05	2.28	3.28	2.06	2.49	3.21	2.01	2.56	2.31	4.02
FeO	14.95	14.75	14.7	11.81	11.9	14.81	13.24	15.34	15.16	16.14	12.21	16.75	13.01
MnO	2.64	2.72	2.81	3.62	4.99	2.87	3.24	3.44	2.51	2.59	4.07	2.73	2.18
MgO	0.63	0.53	0.62	0.15	0.1	0.45	0.21	0.42	0.58	0.4	0.25	0.45	0.44
CaO	20.66	20.76	21.16	23.53	22.59	21.23	22.94	19.98	20.97	20.18	23.73	20.38	23.16
Na_2O	0.1	0.1	0.04	0	0.14	0.15	0.04	0.12	0.08	0.07	0.1	0.03	0.06
K_2O	0	0.08	0	0.01	0.08	0.05	0.07	0.02	0	0.02	0.04	0.04	0.08
Total	100.46	99.52	99.95	99.12	99.44	100.19	99.33	99.99	99.6	99.39	100.98	99.97	100.12
Tsi	6.111	6.072	6.102	6.103	6.106	6.062	6.121	6.061	6.061	6.146	6.079	6.081	6.048
AlVI	3.555	3.502	3.471	3.433	3.534	3.441	3.479	3.565	3.463	3.546	3.542	3.534	3.363
Fe^{3+}	0	0	0	0	0.086	0.113	0.007	0	0.085	0	0.369	0.404	0.77
Ti	0.024	0.031	0.004	0.002	0	0.031	0.012	0.03	0.014	0.026	0.001	0.006	0.026
Cr	0.362	0.399	0.387	0.382	0.286	0.408	0.257	0.309	0.401	0.252	0.317	0.289	0.496
Fe^{2+}	1.957	1.953	1.935	1.565	1.494	1.946	1.744	2.077	2.015	2.139	1.45	2.142	1.78
Mg	0.147	0.125	0.146	0.035	0.024	0.106	0.052	0.1	0.137	0.095	0.058	0.106	0.103
Mn	0.35	0.365	0.375	0.486	0.671	0.382	0.435	0.458	0.336	0.348	0.54	0.367	0.289
Ca	3.464	3.522	3.569	3.994	3.843	3.579	3.886	3.362	3.55	3.427	3.982	3.465	3.878
Na	0.03	0.031	0.012	0	0.043	0.046	0.013	0.037	0.025	0.022	0.03	0.009	0.018
Cations	16	16	16	16	16.08	16.11	16	16	16.08	16	16.37	16.40	16.77
XGrss	0.585	0.59	0.592	0.657	0.637	0.595	0.635	0.561	0.588	0.57	0.66	0.57	0.641
XAlm	0.331	0.327	0.321	0.257	0.248	0.324	0.285	0.346	0.334	0.356	0.24	0.352	0.294
XPyp	0.025	0.021	0.024	0.006	0.004	0.018	0.009	0.017	0.023	0.016	0.01	0.017	0.017
XSpss	0.059	0.061	0.062	0.079	0.111	0.063	0.071	0.076	0.066	0.057	0.089	0.060	0.047
XFe	0.93	0.94	0.93	0.97	0.98	0.95	0.97	0.95	0.94	0.95	0.97	0.96	0.96

* Inclusion in clinopyroxene.

Table 8: Major element content and structural formulae of clinopyroxenes (Cations per 6 oxygen)

Sample	SL1-6	SL1-6	SL1-6	SL1-6	SL1-6	SL1-6	Sl1-8	SL1-8	SL1-8	SL1-8	SL1-8	Sl1-8a	Sl1-8a	Sl1-8a	Sl1-8a	Sl1-8a
SiO_2	52.7	51.56	51.71	51.42	50.99	51.33	52.93	51.78	51.78	51.82	51.12	52.24	52.05	52.69	52.1	52.59	52.52
TiO_2	0	0	0.02	0.16	0.04	0	0.06	0.04	0	0	0	0	0.09	0	0.11	0.22	0.04
Al_2O_3	0.06	0.99	1.02	1.24	1.7	1.14	0.89	0.94	0.41	0.27	1.85	1.15	1.22	0.16	1	1.25	0.99
FeO	9.18	13.17	11.79	11.55	11.61	13.65	10.58	12.29	12.27	12.22	11.27	12.46	12.02	12.1	12.33	11.41	11.39
Cr_2O_3	0.18	0.23	0.29	0.35	0.26	0.32	0.2	0.16	0.49	0.45	0.95	0.24	0.52	0.47	0.44	0.26	0
MnO	0.82	0.69	0.66	0.41	0.47	0.5	0.54	0.38	0.44	0.44	0.41	0.35	0.31	0.21	0.4	0.41	0.49
NiO	0	0.46	0.26	0	0.21	0.31	0	0.13	0.24	0	0	0	0	0	0	0	0
MgO	12.15	9.52	10.15	10.27	10.24	9.42	11.28	10.46	10.29	10.55	10.42	10.34	10.14	10.76	10.25	10.98	10.89
CaO	23.87	23.22	23.25	23.2	23.44	22.92	23.44	23.37	23.11	23.69	23.21	23.24	23	23.66	23.2	22.96	23.26
Na_2O	0.2	0.23	0.44	0.75	0.38	0.36	0.45	0.41	0.38	0.33	0.84	0.45	0.59	0.35	0.48	0.59	0.42
K_2O	0.02	0	0.04	0.06	0.03	0	0	0.01	0.01	0.02	0	0	0.01	0.01	0	0.03	0
Total	99.18	100.07	99.63	99.41	99.37	99.95	100.37	99.97	99.42	99.79	100.07	100.48	99.94	100.43	100.32	100.69	100.01
TSi	2	1.976	1.975	1.959	1.949	1.968	1.992	1.969	1.985	1.977	1.932	1.977	1.979	1.995	1.977	1.976	1.989
TAl	0	0.024	0.025	0.041	0.051	0.032	0.008	0.031	0.015	0.012	0.068	0.023	0.021	0.005	0.023	0.024	0.011
TFe^{3+}	0	0	0	0	0	0	0	0	0	0.011	0	0	0	0	0	0	0
M1Al	0.003	0.02	0.021	0.015	0.025	0.02	0.031	0.011	0.004	0	0.014	0.028	0.034	0.002	0.021	0.031	0.033
M1Ti	0	0	0.001	0.005	0.001	0	0.002	0.001	0	0	0	0	0.003	0	0.003	0.006	0.001
$M1Fe^{3+}$	0.007	0.014	0.029	0.064	0.045	0.029	0	0.043	0.025	0.035	0.087	0.02	0.01	0.014	0.018	0.017	0.006
$M1Fe^{2+}$	0.284	0.401	0.348	0.304	0.326	0.394	0.328	0.343	0.361	0.344	0.269	0.361	0.363	0.362	0.365	0.323	0.345
M1Cr	0.005	0.007	0.009	0.011	0.008	0.01	0.006	0.005	0.015	0.014	0.028	0.007	0.016	0.014	0.013	0.008	0
M1Mg	0.687	0.544	0.578	0.583	0.583	0.539	0.633	0.593	0.588	0.6	0.587	0.583	0.575	0.607	0.58	0.615	0.615
M1Ni	0	0.014	0.008	0	0.006	0.01	0	0.004	0.007	0	0	0	0	0	0	0	0
$M2Fe^{2+}$	0	0.007	0	0	0	0.015	0.005	0.005	0.008	0	0	0	0.013	0.009	0.007	0.009	0.018	0.01
M2Mn	0.026	0.022	0.021	0.013	0.015	0.016	0.017	0.012	0.014	0.014	0.014	0.013	0.011	0.01	0.007	0.013	0.013	0.016
M2Ca	0.971	0.953	0.951	0.947	0.96	0.942	0.945	0.952	0.949	0.968	0.94	0.942	0.937	0.96	0.943	0.924	0.944
M2Na	0.015	0.017	0.033	0.055	0.028	0.027	0.033	0.03	0.028	0.024	0.062	0.033	0.044	0.026	0.035	0.043	0.031
M2K	0.001	0	0.002	0.003	0.001	0	0	0	0	0.001	0	0	0	0	0	0.001	0
Cations	3.999	4	3.998	3.997	3.999	4	4	4	4	3.999	4	4	4	4	4	3.999	4
#Mg	0.7	0.56	0.61	0.61	0.61	0.55	0.66	0.60	0.60	0.61	0.62	0.60	0.60	0.61	0.60	0.63	0.63

Table 9: Major element content and structural formulae of plagioclases (cations per 32 oxygen)

Sample	SL1-6	SL1-6	SL1-6	SL1-6	SL1-6	SL1-6	SL1-8	SL1-8	SL1-8	SL1-8a	SL1-8a	SL1-8a	SL1-8a	SL1-8a	SL1-8a
SiO_2	68.666	67.261	67.524	67.66	68.15	66.92	59.33	59.63	59.46	60.53	60.47	59.81	59.67	59.12	59.05
TiO_2	0	0	0	0	0	0	0	0	0	0	0	0	0	0	0
Al_2O_3	20.01	20.859	19.675	20.81	19.46	20.62	25.66	25.75	25.7	25.63	25.66	26.12	26.37	26.28	26.25
FeO	0.031	0	0.094	0	0.22	0.1	0.06	0	0.05	0	0	0.23	0.14	0.31	0.06
MnO	0	0.229	0.12	0	0	0.16	0	0.08	0	0.16	0.05	0	0.02	0.02	0
MgO	0	0	0	0	0	0	0	0	0	0	0	0	0	0	0
CaO	0.195	1.135	0.507	0.9	0.29	1.36	7.04	7.43	7.22	6.78	7.03	7.72	7.52	7.91	7.52
Na_2O	11.596	11.146	11.601	11.73	12.08	11.35	7.66	7.5	7.35	8.39	8.13	7.86	7.69	7.85	7.3
K_2O	0.058	0	0.104	0.03	0	0.05	0.13	0.14	0.11	0.05	0.1	0.05	0.13	0.07	0.16
Total	100.56	100.63	99.625	101.13	100.2	100.56	99.88	100.5	99.89	101.54	101.44	101.79	101.54	101.56	100.34
Si	11.927	11.722	11.88	11.737	11.922	11.701	10.6	10.59	10.61	10.646	10.642	10.52	10.509	10.445	10.509
Al	4.093	4.281	4.077	4.251	4.009	4.246	5.398	5.386	5.4	5.309	5.318	5.411	5.469	5.468	5.502
Ti	0	0	0	0	0	0	0	0	0	0	0	0	0	0	0
Fe^{2+}	0.005	0	0.014	0	0.032	0.015	0.009	0	0.007	0	0	0.034	0.021	0.046	0.009
Mn	0	0.034	0.018	0	0	0.024	0	0.012	0	0.024	0.007	0	0.003	0.003	0
Mg	0	0	0	0	0	0	0	0	0	0	0	0	0	0	0
Ca	0.036	0.212	0.096	0.167	0.054	0.255	1.347	1.414	1.38	1.278	1.326	1.455	1.419	1.497	1.434
Na	3.906	3.766	3.958	3.945	4.098	3.848	2.653	2.583	2.543	2.861	2.774	2.681	2.626	2.689	2.519
K	0.013	0	0.023	0.007	0	0.011	0.03	0.032	0.025	0.011	0.022	0.011	0.029	0.016	0.036
Cations	19.98	20.015	20.066	20.107	20.115	20.1	20.04	20.02	19.97	20.129	20.089	20.112	20.076	20.164	20.009
Xab	0.99	0.95	0.98	0.96	0.99	0.94	0.66	0.65	0.65	0.69	0.68	0.65	0.65	0.64	0.64
Xan	0.01	0.05	0.02	0.04	0.01	0.06	0.34	0.35	0.35	0.31	0.32	0.35	0.35	0.36	0.36

Table 10: Major element content and structural formulae of epidotes (cations per 12.5 oxygen)

Sample	SL1-6	SL1-6	SL1-6	SL1-6	SL1-6	SL1-6	SL1-8	SL1-8	SL1-8	SL1-8	SL1-8	SL1-8	SL1-8	SL1-8	SL1-8	SL1-8
Variety	3	3	2	2	1	1	1	1	1	1	1	2	2	1	1	1
SiO_2	38.96	38.304	38.33	38.83	37.74	37.5	39.27	38.76	38.61	38.92	39.13	38.58	38.89	38.79	39.13	38.4
TiO_2	0.36	0	0.09	0.03	0.09	0.18	0.19	0.17	0.27	0.28	0.21	0.08	0.17	0.24	0.27	0.23
Al_2O_3	28.75	25.994	26.15	26.4	22.76	21.87	28.24	27.28	28.64	27.48	28.19	25.81	26.04	26.81	28.43	27.27
FeO	4.85	8.02	7.75	7.95	9.74	12.05	6.89	6.95	5.13	6.49	6.92	8.28	7.44	6.89	5.85	6.58
Cr_2O_3	0.71	0	1.4	0.81	2.66	2.17	0.54	0.89	0.47	0.79	0.55	1.29	1.27	1.54	1.05	0.92
MnO	0.06	0.16	0.08	0.34	0.19	0.05	0	0.03	0.26	0.21	0	0.2	0.15	0.11	0.16	0.02
MgO	0	0	0	0	0	0.05	0	0	0	0.04	0.07	0	0.03	0.06	0	0.08
CaO	23.81	23.478	23.65	23.53	23.09	22.97	23.86	23.81	23.64	23.47	23.61	23.46	23.44	23.82	23.98	23.44
Na_2O	0.08	0	0.2	0	0.16	0.27	0.05	0	0.02	0.09	0.02	0.1	0.1	0	0	0.07
K_2O	0.04	0.036	0.02	0.04	0.01	0.03	0.07	0	0	0	0.03	0.06	0	0	0	0.04
Total	97.62	95.585	97.67	97.93	96.44	97.14	99.12	97.89	97.05	97.77	98.73	97.85	97.53	98.26	98.87	97.05
Si	3.008	3.031	2.994	3.018	3.018	2.993	2.999	3.003	3.001	3.014	2.997	3.009	3.033	3.002	2.994	2.999
AlIV	0	0	0.006	0	0	0.007	0.001	0	0	0	0.003	0	0	0	0.006	0.001
AlVI	2.614	2.423	2.4	2.416	2.144	2.048	2.538	2.489	2.621	2.506	2.54	2.371	2.391	2.443	2.556	2.507
Ti	0.021	0	0.005	0.002	0.005	0.011	0.011	0.01	0.016	0.016	0.012	0.005	0.01	0.014	0.016	0.014
Cr	0.043	0	0.086	0.05	0.168	0.137	0.033	0.054	0.029	0.048	0.033	0.079	0.078	0.094	0.063	0.057
Mn	0.004	0.011	0.005	0.022	0.013	0.003	0	0.002	0.017	0.014	0	0.013	0.01	0.007	0.01	0.001
Mg	0	0	0	0	0	0.006	0	0	0	0.005	0.008	0	0.003	0.007	0	0.009
Ca	1.97	1.991	1.979	1.959	1.979	1.964	1.952	1.977	1.969	1.948	1.938	1.96	1.958	1.975	1.966	1.961
Na	0.012	0	0.03	0	0.025	0.042	0.007	0	0.003	0.014	0.003	0.015	0.015	0	0	0.011
K	0.004	0.004	0.002	0.004	0.001	0.003	0.007	0	0	0	0.003	0.006	0	0	0	0.004
Fe^{3+}	0.31	0.53	0.51	0.52	0.65	0.8	0.44	0.45	0.33	0.42	0.44	0.54	0.48	0.45	0.37	0.43
Cations	7.986	7.99	8.017	7.991	8.003	8.014	7.988	7.985	7.986	7.985	7.977	7.998	7.978	7.992	7.981	7.994
Ps	0.11	0.18	0.17	0.18	0.23	0.28	0.15	0.15	0.11	0.14	0.15	0.19	0.17	0.16	0.13	0.15

Sample BE1

In this rock, clinopyroxene does not record any zonation. Compared to the samples described above, the grains have a much higher Mg/Fe ratio, and their Mg/(Mg+Fe) ratio ranges between 0.77-0.79. The Ca-concentration varies between 0.95 and 0.97 a.p.f.u. Although this sample does not contain epidote, the clinopyroxenes show the same irregularities with respect to their Al concentration. The

plagioclase grains show a relatively wide range in compositions with two extreme values for Xan of 0.33 and 0.46, respectively. Most of the measurements scatter around 0.36-0.4 within single grains. The amphibole grains record Mg/(Mg+Fe) ratios of 0.69-0.71, and have Ca concentrations between 1.90-1.96.

QUANTIFYING THE METAMORPHIC CONDITIONS

As has been shown by Spear et al. (1991), the only effective means for plagioclase to equilibrate in response to changing PT- conditions is to dissolve old plagioclase and precipitate new plagioclase, as diffusion rates within the crystal are known to be very slow (Grove et al., 1984). For rocks with a Ca-rich bulk composition, any prograde metamorphism will result in the consumption of the Ca-rich phases such as epidote, zoisite and calcite and the production of a grossular component in garnet and an anorthite component in plagioclase (Spear, 1993). In cases where plagioclase is the only remaining Ca-source, garnet-forming reactions will consume the anorthite component in plagioclase. The epidote inclusions in peak metamorphic clinopyroxene indicate that epidote and quartz were present on the prograde path to form grossular and anorthite. The absence of prograde epidote, other than as inclusions, suggests that the garnet-forming reaction during late prograde and peak metamorphic evolution was:

$$\textbf{Clinopyroxene + Anorthite} \quad \textbf{Grossular + Almandine + Quartz} \qquad \textbf{(1)}$$

The replacement of garnet by epidote during the retrogression of the metasediments is interpreted to have consumed the grossular component in garnet and the anorthite component in plagioclase via the reaction:

$$\textbf{Anorthite + Grossular + H}_2\textbf{O} \quad \textbf{Epidote + Quartz} \qquad \textbf{(2)}$$

Figure 15 illustrates the predicted mineral chemical changes in response to this reaction. The commonly observed association of sphene with this retrograde assemblage further indicates that reaction (2) was coupled with another anorthite-consuming reaction, such as:

$$\textbf{Hedenbergite + Anorthite + Ilmenite} \quad \textbf{Grossular + Almandine + Sphene} \qquad \textbf{(3)}$$

Reaction (3) has been used for geobarometry (Mukhopadhyay et al., 1992), but cannot be applied in this study, because no ilmenite has been identified.

Estimation of the Peak Metamorphic PT Conditions

Several conventional geothermobarometers have been applied to the clastic metasediments, amphibolites and banded iron formation. The PT locations of the relevant univariant equilibria used for geobarometry were calculated with the program THERMOCALC, using the self-consistent thermodynamic dataset of Holland and Powell (1998), and the activity models listed in Table 11. Data obtained for the clastic metasediments using the average PT-method are in agreement with the results presented below, but give relatively large errors for the estimated temperatures. The geothermometers, in general, give relatively consistent results ranging between 600-750C (Fig. 16), but the estimated temperatures for the metasediments tend to be consistently higher than the temperatures estimated for both amphibolites and banded iron formation. The estimation of the peak metamorphic pressures was problematic and required a detailed investigation of the chosen mineral compositions as well as the methods used.
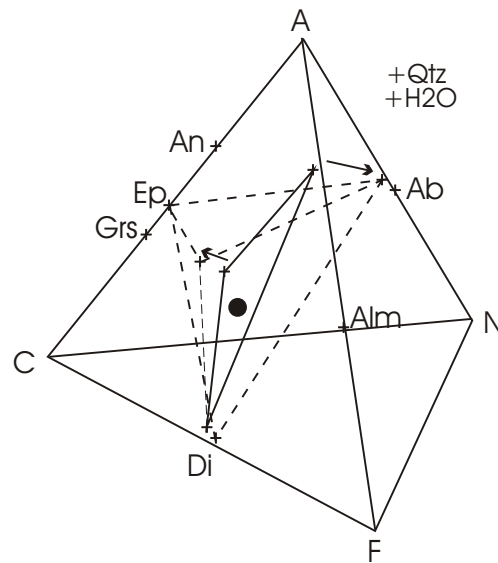
Figure 15: *ACFN-diagram illustrating the geochemical changes in response to reaction (2). The formulae used to calculate the coordinates are from Spear (1993). Normal tie lines connect the peak metamorphic minerals garnet, diopside and anorthite. The dashed tie lines connect retrograde phases, including the garnet (rims), diopside, albite and epidote, the filled circle represents the bulk composition.*
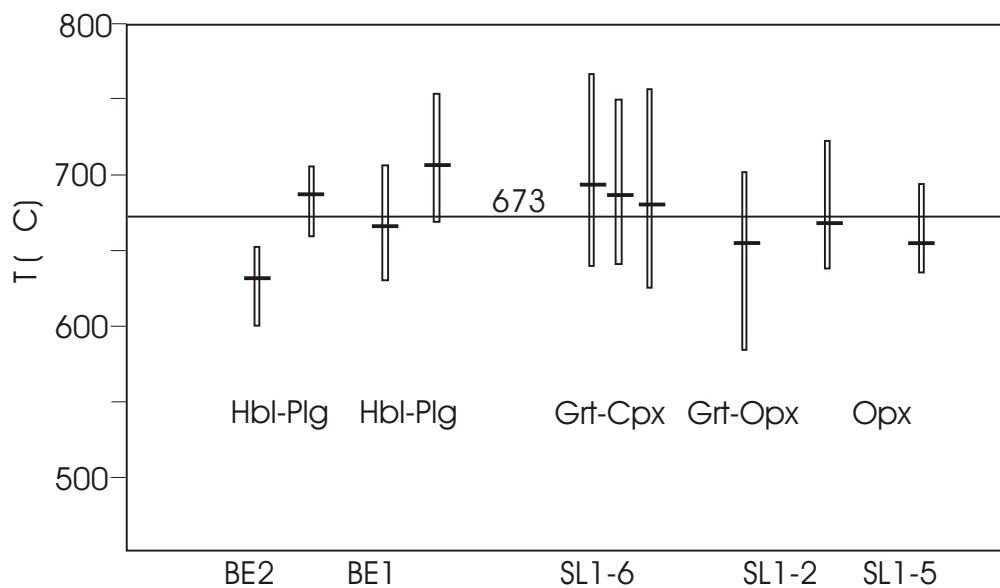

Figure 16: *Plot of the estimated peak metamorphic temperatures and temperature average using the Hbl-Plg, Grt-Cpx, Grt-Opx and Opx-thermometer. The first bar for sample BE 2 and BE 1 corresponds to the reaction edenite + quartz = tremolite + albite, the second bar to the reaction edenite + albite = richterite + anorthite. From left to right, the 3 bars for the Grt-Cpx thermometry are temperature estimates using the calibration from Ellis and Green (1979), Ganguly (1979) and Powell (1985). Temperature estimates using the Grt-Opx thermometer have been calculated after Harley (1984a), where Fe^{3+} is estimated by mass balance. The Opx thermometer (Witt-Eickschen and Seck, 1991) is based on the solubility of Ca-Al and Cr-Al in orthopyroxene.*

Geothermometers

Garnet-Cpx Thermometry - The three different calibrations for the reaction $Fe_3Al_2Si_3O_{12}$ + $3CaMgSi_2O_6$ $Mg_3Al_2Si_3O_{12}$ + $3CaFeSi_2O_6$ of Ellis and Green (1979), Ganguly (1979) and Powell (1985) are considered to give realistic temperature estimates in these rocks. Only those garnet cores have been used that are believed to give the best estimate for the peak metamorphic garnet compositions. However, the difference between the relatively Ca-depleted and Fe-enriched cores from extensively altered garnet grains and those grains that do not show any replacement is relatively small. For sample SL1-6, the three calibrations give almost identical results averaging around 686 º C.

Hornblende-Plagioclase Thermometer -The Hb-Plg thermometer (Holland and Blundy, 1994) has been applied to two samples. Two reactions have been used i.e., edenite + quartz tremolite + albite and edenite + albite richterite + anorthite. Sample BE 2 is a medium-grained amphibolite with the assemblage hornblende + plagioclase + quartz, and sample BE 1 is a medium-grained metasediment with the assemblage hornblende + plagioclase + diopside + quartz. The temperature estimates at a set pressure of 10 kbar are shown in Figure 16. The edenite-richterite thermometer yields consistently higher results at these pressures, but the differences in the estimated temperatures are within the given error of 40 º C for sample BE 1. In general, reaction 1 has a positive slope (temperature decreases with increasing pressure), whereas reaction 2 has a negative slope in PT space.

Garnet-Orthopyroxene Thermometer - Garnet-orthopyroxene geothermometry and geobarometry (Harley, 1984a,b) has been widely used to estimate PT conditions in high-grade metamorphic terranes. The successful application of the garnet-orthopyroxene thermometer to garnetiferous banded iron formation is limited by several factors, including the generally limited precision at lower (e.g., amphibolite facies grade) temperatures (Harley, 1984a), the effect of the bulk rock Fe-content (Carson and Powell, 1997) and the resulting uncertainty in estimating ferric iron. In addition, Harley (1984a) questioned the reliability of the grt-opx thermometer when applied to metamorphosed iron formation, as the Mn-concentrations in garnets are commonly high (e.g., Xspss > 0.04). The investigated sample contains garnets with a Xspss 0.04. Despite the relatively large error, the calculated temperatures, although slightly lower, are consistent when compared to the other temperature estimates.

Orthopyroxene Thermometer - This empirical geothermometer was calibrated for spinel peridotites with a buffering mineral assemblage of orthopyroxene, clinopyroxene, spinel and olivine (Witt-Eickschen and Seck, 1991), and is based on the solubility of Ca-Al and Cr-Al in orthopyroxene.

Geobarometers

Garnet-Clinopyroxene-Plagioclase-Quartz Barometer - As the end-member reaction hedenbergite + anorthite grossular + almandine + quartz is the reaction interpreted to have produced the peak metamorphic mineral assemblage in the clastic metasediments, this barometer is readily applicable to these rocks. The two calibrations of Powell and Holland (1988) and Eckert et al. (1991) give similar results for the estimated pressures for all three samples although the pressures obtained from the calibration of Eckert et al. (1991) are systematically higher (Fig. 17). The locations of this univariant reaction calculated from the compositions of the peak metamorphic minerals in sample SL1-6, SL1-8 and SL1-8a are plotted in Figure 18. For sample SL1-6, where only retrograde albite has been identified, the peak plagioclase compositions are assumed to have been identical to those of other metasediments in which andesine is still preserved.
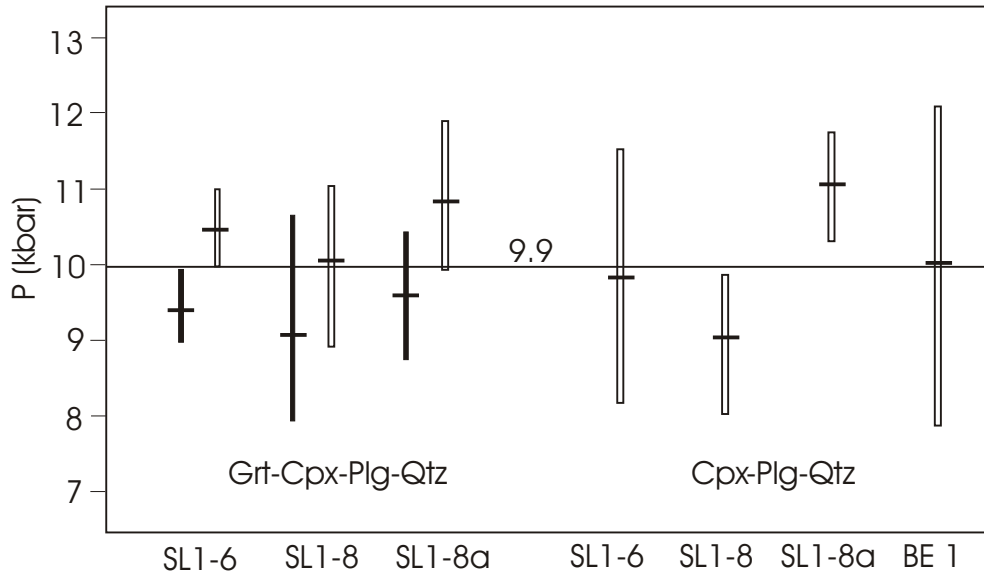
Figure 17: *Plot of the estimated pressures and pressure average using the Grt-Cpx-Plg-Qtz barometer (Powell and Holland, 1988; Eckert et al., 1991) and the Cpx-Plg-Qtz barometer (Ellis, 1980). On average, the pressure estimates using the calibration of Eckert et al. (1991) for the Grt-Cpx-Plg-Qtz barometer are about 1 kbar higher than pressures calculated from Powell and Holland (1988).*
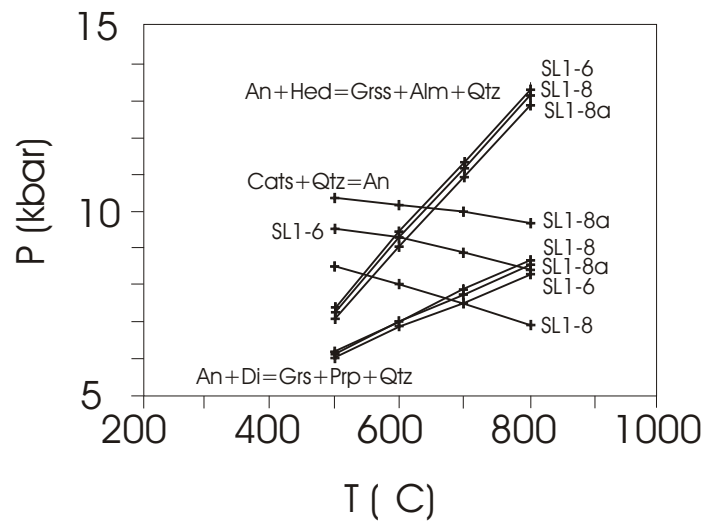

Figure 18: *Calculated curves for pressure-sensitive univariant equilibria for the end-member reactions hedenbergite + anorthite grossular + almandine + quartz, CaTs + quartz anorthite, and anorthite + diopside grossular + pyrope + quartz. The activities used for calculating the equilibria are average values for the respective minerals, except for Cpx, where mineral analyses with CaTs activities < 0.042 were chosen.*

Plagioclase-Clinopyroxene-Quartz Barometer - The Plg-Cpx-Qtz barometer was calibrated for the reaction $CaAl_2Si_2O_8$ $CaAl_2SiO_6 + SiO_2$ (anorthite = Ca Tschermaks molecule + quartz). The application of this barometer (Ellis, 1980) to our samples was somewhat problematical due to the generally low and variable Al concentrations in clinopyroxene and the resulting differences in the activity values for the Ca Tschermaks Molecule (CaTs). Al concentrations in clinopyroxene are considerably reduced where in contact with or partially replaced by epidote. Thus, the use of this barometer is reliant on identifying peak metamorphic Al concentrations in clinopyroxene. After identifying suitable clinopyroxene compositions, great care is still required due to the low Al-concentrations and the fact that the CaTs activities are based on alumina situated in the M1 site.

Thus, it is highly sensitive to analyses with erroneously low Si totals. In this study a silica concentration of 1.96-1.98 pfu. was chosen as a reliable estimate of the Si content of peak metamorphic clinopyroxene. Despite this approach the clinopyroxenes still have quite variable CaTs activities with values ranging between 0.023-0.079, which are equivalent to a pressure span of about 8-16 kbar. Propagation of the errors connected with the measurements of Al in clinopyroxene via probe analyses, and propagation of this error through the CaTs activities, revealed that the range in the activities calculated may potentially be ascribed to the inherent uncertainties of the probe data. This is a function of the low Al concentrations in this mineral. CaTs activities of greater than 0.042 give erroneously high values of greater than 12 kbar, as indicated by the small jadeite component in Cpx and the occurrence of muscovite as a stable peak metamorphic phase in some of the arkoses. Pressures calculated from CaTs activities between 0.023 and 0.042 are very similar to the pressure estimates using the Grt-Cpx-Plg-Qtz barometer. The majority of our peak metamorphic clinopyroxene compositions fall into this category.

Table 11: Activity models used for calculating the location of the univariant equilibria shown in Figure 17

Endmember	Thermodynamic mole fraction	Activity model
Albite	$X_{Ab} = (1-X_{Ca})$	Ideal mixing, ordered
Anorthite	$X_{An} = X_{Ca}$	Holland and Powell, 1992
Grossular	$X_{Grs} = (X_{Ca})^3(X_{Al})^2$	Ideal 2 site mixing,
Almandine	$X_{Alm} = (X_{Fe})^3(X_{Al})^2$	regular solution gammas
Spessartin	$X_{Spss} = (X_{Mn})^3(X_{Al})^2$	
Pyrope	$X_{Pyp} = (X_{Mg})^3(X_{Al})^2$	
Andradite	$X_{Adr} = (X_{Ca})^3(X_{Fe}^{3+})^2$	
Diopside	$X_{Di} = X_{Ca,M2}X_{Mg,M1}$	Ideal 2 site mixing,
Hedenbergite	$X_{Hed} = X_{Fe,M1}X_{Ca,M2}$	disordered
CaTs	$X_{Cats} = X_{Al,M1}X_{Ca,M2}$	regular solution gammas

Retrograde PT Conditions

Retrogression in the rock types studied has produced the typical greenschist facies minerals actinolite, grunerite, albite and epidote. Although most of the peak metamorphic mineral assemblages were replaced by hydrous phases, the degree to which replacement occurs differs between samples. This is interpreted to reflect the fact that H_2O availability was a limiting factor in reaction progress. Equilibration during the retrogression event appears to have been poor. This is perhaps best demonstrated by the clastic metasediments where retrogression has produced the assemblage Grt-rim + Ep + Ab + Qtz + Cpx. Both garnet and clinopyroxene show mineral composition changes where in contact with the retrograde epidote. However, the observed changes, e.g., the increase in the grossular component of garnet, do not follow a systematic spatial pattern with respect to the epidote-garnet contact (Fig. 12) and there are strong variations of the Ca:Al ratios in garnet rim compositions and epidote (Fig. 19). This is interpreted to reflect disequilibrium during the reaction of garnet to epidote resulting from the very slow rate of diffusion in garnet, even at amphibolite facies conditions (Chernoff and Carlson, 1999). Calculations by Spear (1988) indicate that the time scale required to partially or completely homogenize even small garnets at temperatures between 600-750C is tens of millions of years. An additional reason for the observed garnet-epidote compositional relationship may be the very localized changes in the stoichiometry of the garnet breakdown reaction resulting from the consumption of the anorthite component in plagioclase. Assuming that anorthite reacted out through reaction/s (2) and/or (3) at some point during retrogression, and taking the simplified mineral formulae as shown in Table 4 with a Ca:Al ratio of approximately 1:1 in garnet and 1:1.25 in epidote, further progressive replacement of garnet

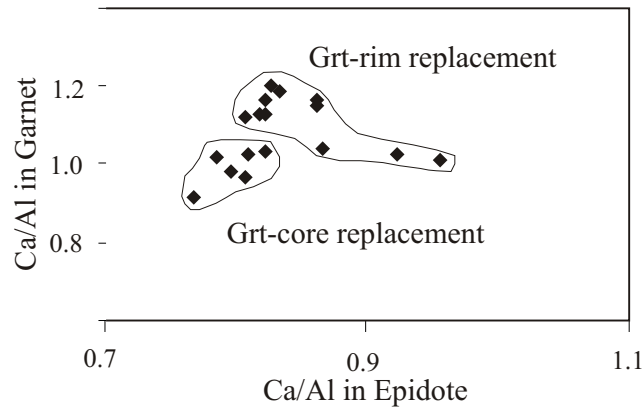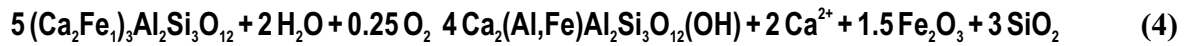by epidote would produce an excess of Ca in garnet via the reaction:

$$5\,(Ca_2Fe_1)_3Al_2Si_3O_{12} + 2\,H_2O + 0.25\,O_2 \quad 4\,Ca_2(Al,Fe)Al_2Si_3O_{12}(OH) + 2\,Ca^{2+} + 1.5\,Fe_2O_3 + 3\,SiO_2 \qquad (4)$$

Figure 19: Plot of the Ca:Al ratio in garnet and epidote.

Thus, although the partitioning of Ca between garnet and plagioclase has been shown to be a strong function of pressure (e.g., Kohn et al., 1992), the results presented above indicate that chemical equilibrium between these minerals was probably never reached during retrogression in these rocks. This is also reflected by the average pressure-temperature calculations using the retrograde assemblage Grt-rim + plagioclase (Xan 0.09) + epidote + quartz + clinopyroxene, which indicate isothermal loading during retrogression up to a pressure of 20 kbar. This is obviously incorrect, as the rocks contain none of the characteristic high-pressure phases that would have been produced at these pressures.

IMPLICATIONS

The data presented in this study give some important insights into the evolution of the lower portions of the Onverwacht Group. The controversy concerning the exact age of the Theespruit Formation and its relative position to the overlying Komati Formation has led some authors to suggest that it represents an active convergent margin sequence (e.g., Armstrong et al., 1990, de Ronde and de Wit, 1994). Kröner et al. (1996), however, favoured a setting similar to an oceanic plateau due to the lack of andesitic compositions and trench-like sediments. The geochronological data show that the deposition of the clastic sediments must have occurred during a very short period of time, contemporaneously with the erosion of spatially associated older granitoid rocks. Shortly after, the southern part of the Barberton greenstone belt was exposed to intense calc-alkaline magmatic activity, which resulted in the *c.* 3445 Ma TTG plutonism and the formation of high- level equivalents in the Hooggenoeg Formation (e.g., de Wit et al., 1987a). We therefore suggest that the lowermost formations of the Onverwacht Group, both the Theespruit and Sandspruit Formations, represent rocks formed in a tectonically and magmatically active environment, comparable to modern accretionary wedges in a continental margin or arc setting. At this time, the trondhjemite plutons intruded at relatively shallow crustal levels and the related volcaniclastic rocks were laid down on top of the closely associated Komati Formation.

The peak metamorphic PT conditions in the study area are considerably higher than anything reported so far from the Barberton greenstone belt and are well within the stability field for kyanite (Fig. 20). Stevens et al. (in prep.) estimated the peak-metamorphic pressure-temperature conditions for the Schapenburg schist belt, some 20 km further south of the study area, to be $623 \pm 35\,^{\circ}C$ and 6.0 ± 1.3 kbar. This suggests higher temperatures and pressures in the granite-greenstone terrane approaching the main body of the Barberton greenstone belt. Despite this pressure-gradient, there is
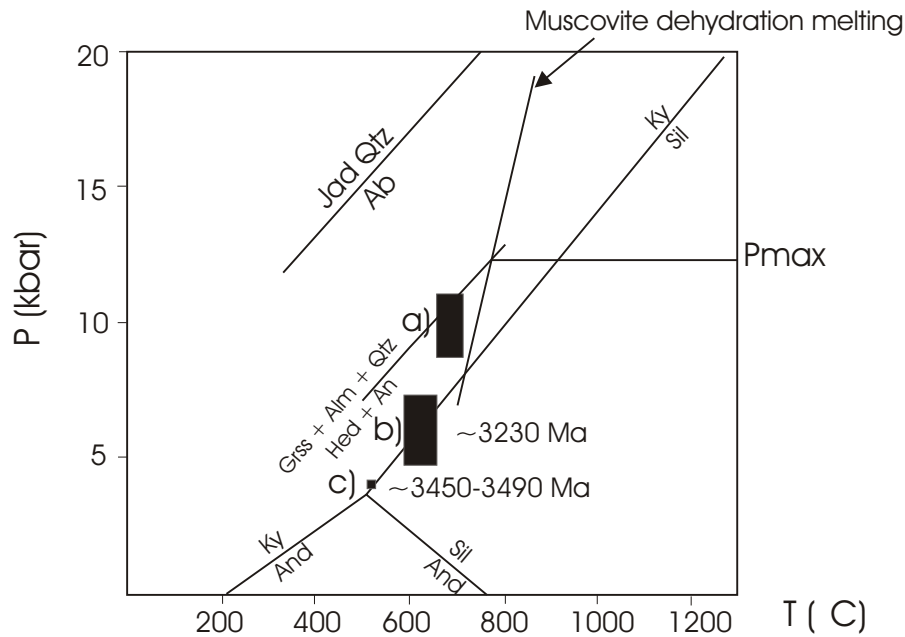
Figure 20: *PT diagram summarising the average peak metamorphic PT conditions: (a) from this study compared to results from (b) Stevens et al. (in prep.) and (c) Cloete (1991). A maximum pressure of about 12 kbar is given by the interception of the univariant equilibria plotted in Figure 14 and the muscovite dehydration melting curve of Petö (1976), because muscovite forms a stable peak metamorphic phase in some of the samples investigated. Therefore, any pressure estimate higher than 12 kbar using conventional geobarometry has not been included. The reaction Albite Jadeite + Quartz has been determined experimentally by Holland (1980). The alumino-silicate phase diagram is after Holdaway (1971).*

strong evidence that one single tectono-metamorphic event was responsible for the peak of metamorphism atSchapenburg and the greenstone remnants investigated in this study. This includes:

1.	the continuation of the tectonic fabric from the Schapenburg schist belt into the greenstone remnants investigated in this study (Fig. 3);
2.	in both areas, the peak metamorphic garnets are completely equilibrated at the metamorphic peak, so that any record of the prograde PT path has been obscured; and
3.	U-Pb data on metamorphic sphenes and zircons from a foliated trondhjemite phase of the Stolzburg pluton, give age estimates at 3201, 3237 and 3255 Ma (Kamo and Davis, 1994, Fig. 1), and correlate well with the U-Pb zircon age of *c.* 3231 ± 5 Ma found for a syntectonic intrusion at Schapenburg (Stevens et al., in prep.).

Therefore, the peak metamorphic mineral assemblages in these rocks equilibrated during a major metamorphic event, which correlates with the main compressional event in Barberton region as a whole. Because the prograde PT path is no longer preserved, the cause for crustal thickening cannot be established by metamorphic means. However, the maximum pressures of 7-11 kbar indicate a (minimum) crustal thickness of approximately 30 km for the granite-greenstone terrane south of the Barberton greenstone belt, which is comparable to the base of modern orogenic belts. Although the present database makes it difficult to interpret the PT evolution of these rocks, there is evidence from the Onverwacht Group in the main belt (e.g., de Wit, 1982, 1991), and from Schapenburg (Stevens et al., in prep.), that the crustal thickening in this area involved thrusting. The results presented above further imply that the granite-greenstone terrane to the south of the Barberton greenstone belt, although younger in age than the rocks of the Onverwacht Group, represents a basement relative to the Barberton greenstone belt at the time of peak metamorphism.

ACKNOWLEDGEMENTS

REFERENCES

Anhaeusser, C.R., 1969. The stratigraphy, structure and gold mineralization of the Jamestown and Sheba Hills area of the Barberton Mountain Land. Ph.D. thesis (unpubl.), Univ. Witwatersrand, Johannesburg, 332 pp.

Anhaeusser, C.R., 1973. The evolution of the early Precambrian crust of southern Africa. Phil. Trans. R. Soc. Lond., A 273: 359-388.

Anhaeusser, C.R., 1975. Precambrian tectonic environments. Ann. Rev. Earth Planet. Sci., 3: 31-53.

Anhaeusser, C.R., 1980. A geological investigation of the Archaean granite-greenstone terrane south of the Boesmanskop syenite pluton, Barberton Mountain Land. Trans. Geol. Soc. S. Afr., 83: 93-106.

Anhaeusser, C.R., 1983. The geology of the Schapenburg greenstone remnant and surrounding Archaean granitic terrane south of Badplaas, eastern Transvaal. Spec. Publ. Geol. Soc. S. Afr., 9: 31-44.

Anhaeusser, C. R., 1984. Structural elements of Archaean granite-greenstone terranes as exemplified by the Barberton Mountain Land, southern Africa. In: A. Kröner and R. Greiling (Eds.), Precambrian Tectonics Illustrated. E. Schweizerbart'sche Verlagsbuchhandlung (Nägele u. Obermiller), Germany, Stuttgart, pp. 57-78.

Anhaeuser, C.R. and Robb, L.J., 1980. Regional and detailed field and geochemical studies of Archaean trondhjemitic gneisses, migmatites and greenstone xenoliths in the southern part of the Barberton mountain land, South Africa. Precambrian Res., 11: 373-397.

Anhaeusser, C. R. and Robb, L.J., 1981. Magmatic cycles and the evolution of the Archaean granitic crust in the Eastern Transvaal and Swaziland. Spec. Publ. Geol. Soc. Aust., 7: 457-467.

Anhaeusser, C. R., Robb, L.J. and Barton, J.M. Jr., 1983. Mineralogy, petrology and origin of the Boesmanskop syeno-granite complex, Barberton Mountain Land, South Africa. Spec. Publ. Geol. Soc. S. Afr., 9: 169-183.

Anhaeusser, C.R., Robb, L.J. and Viljoen, M.J., 1983. Notes on the provisional geological map of the Barberton greenstone belt and surrounding granitic terrane, eastern Transvaal and Swaziland (1:250 000 colour map). Trans. Geol. Soc. S. Afr., 9: 221-223.

Armstrong, R.A., Compston, W., de Wit, M.J. and Williams, I.S., 1990. The stratigraphy of the 3.5-3.2 Ga Barberton greenstone belt revisited; a single zircon ion microprobe study. Earth Planet. Sci. Lett., 101 (1): 90-106.

Carson, C.J. and Powell, R., 1997. Garnet-orthopyroxene geothermometry and geobarometry: error propagation and equilibration effects. J. Metamorphic Geol., 15: 679-686.

Chernoff, C.B. and Carlson, W.D., 1999. Trace element zoning as a record of chemical disequilibrium during garnet growth. Geology, 27: 555-558.

Cloete, M., 1991. An overview of metamorphism in the Barberton greenstone belt, 85-98. In: L. D. Ashwal, (Editor), Two Cratons and an Orogen Excursion Guidebook and Review Articles for a Field Workshop through Selected Archaean Terranes of Swaziland, South Africa and Zimbabwe. IGCP Project 280, Dept. of Geology, Univ. Witwatersrand, Johannesburg, 312pp.

Cloete, M., 1999. Aspects of volcanism and metamorphism of the Onverwacht Group lavas in the southwestern portion of the Barberton greenstone belt. Mem. Geol. Surv. S. Afr., 84: 232 pp.

Compston, W., Williams, I.S., Kirschvink, J.L., Zhang, Z. and Ma, G., 1992. Zircon U-Pb ages for the early Cambrian time-scale. J. Geol. Soc. Lond., 149: 171-184.

De Ronde, C.E.J. and de Wit, M.J., 1994. Tectonic history of the Barberton greenstone belt, South Africa; 490 million years of Archaean crustal evolution. Tectonics, 13 (4): 983-1005.

De Ronde, C.E.J. and Kamo, S.L., 2000. An Archaean arc-arc collisional event: a short-lived (ca 3 Myr) episode, Weltevreden area, Barberton greenstone belt, South Africa. J. Afr. Earth Sci., 2: 219-248.

De Ronde, C.E.J., Kamo, S., Davis, D.W., de Wit, M.J. and Spooner, E.T.C., 1991. Field, geochemical and U-Pb isotopic constraints from hypabyssal felsic intrusions within the Barberton greenstone belt, South Africa: implications for tectonics and the timing of gold mineralization. Precambrian Res., 49: 261-280.

De Wit, M.J., 1982. Gliding and overthrust nappe tectonics in the Barberton greenstone belt. J. Struct. Geol., 4 (2): 117-136.

De Wit, M.J., 1991. Archaean greenstone belt tectonism and basin development: some insights from the Barberton and Pietersburg greenstone belts, Kaapvaal Craton, South Africa. J. Afr. Earth Sci., 13 (1): 45-63.

De Wit, M.J., Armstrong, R.A., Hart, R.J. and Wilson, A.H., 1987a. Felsic igneous rocks within the 3.3- to 3.5-Ga Barberton greenstone belt: high crustal level equivalents of the surrounding tonalite-trondhjemite terrain, emplaced during thrusting. Tectonis, 5: 529-549.

De Wit, M.J., Hart, R.A. and Hart, R.J., 1987b. The Jamestown ophiolite complex, Barberton mountain belt; a section through 3.5 Ga oceanic crust. J. Afr. Earth Sci., 6 (5): 681-730.

Eckert, J.O., Newton, R.C. and Kleppa, O.J., 1991. The H of reaction and recalibration of garnet-pyroxene-plagioclase-quartz geobarometers in the CMAS system by solution calorimetry. Amer. Mineral., 76: 148-160.

Ellis, D.J., 1980. Osumilite-sapphirine-quartz granulites from Enderby Land, Antarctica: P-T conditions of metamorphism, implications for garnet-cordierite equilibria and the evolution of the deep crust. Contrib. Mineral. Petrol., 74: 201-210.

Ellis, D.J. and Green, E.H., 1979. An experimental study of the effect of Ca upon garnet-clinopyroxene Fe-Mg exchange equilibria. Contrib. Mineral. Petrol., 71: 13-22.

Ganguly, J., 1979. Garnet and clinopyroxene solid solutions and geothermometry based on Fe-Mg distribution coefficient. Geochim. Cosmochim. Acta, 43: 1021-1029.

Grove, T.L., Baker, M.B. and Kinzler, R.J., 1984. Coupled CaAl-NaSi diffusion in plagioclase feldspar: experiments and applications to cooling rate speedometry. Geochim. Cosmochim. Acta, 48: 2113-2121.

Harley, S.L., 1984a. An experimental study of the partitioning of Fe and Mg between garnet and orthopyroxene. Contrib. Mineral. Petrol., 86: 359-373.

Harley, S.L., 1984b. The solubility of alumina in orthopyroxene coexisting with garnet in FeO-MgO-Al$_2$O$_3$-SiO$_2$ and CaO-FeO-MgO-Al$_2$O3-SiO$_2$. J. Petrol., 25 (3): 665-696.

Harris, P.D., Robb, L.J. and Tomkinson, M.J., 1993. The nature and structural setting of rare-element pegmatites along the northern flank of the Barberton greenstone belt, South Africa. Inform. Circ. Econ. Geol. Res. Unit, Univ. Witwatersrand, Johannesburg, 261: 28pp.

Holdaway, M.J., 1971. Stability of andalusite and the aluminum phase diagram. Amer. J. Sci., 271: 97-131.

Holland, T.J.B., 1980. The reaction albite = jadeite + quartz determined experimentally in the range 600-1200C. Amer. Mineral., 65: 129-134.

Holland, T.J.B. and Powell, R., 1992. Plagioclase feldspars: activity-composition relations based upon Darken`s quadratic formalism and Landau theory. Amer. Mineral., 77, 53-61.

Holland, T.J.B. and Blundy, J., 1994. Non-ideal interactions in calcic amphiboles and their bearing on amphibole-plagioclase thermometry. Contrib. Mineral. Petrol., 116: 433-447.

Holland, T.J.B. and Powell, R., 1998. An internally consistent thermodynamic dataset for phases of petrological interest. J. Metamorphic Geol., 16: 309-343.

Kamo, S.L. and Davis, D.W., 1994. Reassessment of Archaean crustal development in the Barberton Mountain Land, South Africa, based on U-Pb dating. Tectonics, 13 (1): 165-192.

Kisters, A.F.M. and Anhaeusser, C.R., 1995a. The structural significance of the Steynsdorp pluton and anticline within the tectono-magmatic framework of the Barberton Mountain Land. S. Afr. J. Geol., 98(1): 43-51.

Kisters, A.F.M. and Anhaeusser, C.R., 1995b. Emplacement features of Archaean TTG plutons along the southern margin of the Barberton greenstone belt, South Africa. Precambrian Res., 75: 1-15.

Kohn, M.J., Orange, D.L., Spear, F.S., Rumble, D. and Harrison, T.M., 1992. Pressure, temperature, and structural evolution of west-central New Hampshire: hot thrusts over cold basement. J. Petrol., 33: 521-556.

Kretz, R., 1983. Symbols for rock-forming minerals. Amer. Mineral., 68: 277-279.

Krogh, T.E., 1982. Improved accuracy of U-Pb ages by the creation of more concordant system using an air abrasion technique. Geochim. Cosmochim. Acta, 46: 617-649.

Kröner, A. and Compston, W., 1988. Ion microprobe ages of zircons from early Archaean granite pebbles and greywacke, Barberton greenstone belt, southern Africa. Precambrian Res., 38: 367-380.

Kröner, A., and Todt, W., 1988. Single zircon dating constraining the maximum age of the Barberton greenstone belt, South Africa. J. Geophys. Res., 93 (B12): 15 329-15 337.

Kröner, A., Hegner, E., Wendt, J.I. and Byerly, G.R., 1996. The oldest part of the Barberton granitoid-greenstone terrain, South Africa, evidence for crust formation between 3.5 and 3.7 Ga. Precambrian Res., 78: 105-124.

Lancelot, J., Vitrac, A. and Allegre, C.J., 1976. Uranium and lead isotopic dating with grain by grain zircon analysis: a study of complex geological history with a single rock. Earth Planet. Sci. Lett., 29: 357-366.

Leake, B.E., Wooley, A.R., Arps, C.E.S., Birch, W.D., Gilbert, M.C., Grice, J.D., Hawthorne, F.C., Kato, A., Kisch, H.J., Krivovichek, V.G., Linthout, K., Laird, J., Mandarino, J., Maresch, W.V., Nickel, E.H., Rock, N.M.S., Schumacher, J.C., Smith, D.C., Stephenson, N.C.N., Ungaretti, L., Whitaker, E.J.W. and Youzhi, G., 1997. Nomenclature of amphiboles, report of the Subcommittee on Amphiboles of the International Mineralogical Association Commission on New Minerals and Mineral Names. European J. Mineral., 9 (3): 623-651.

Lopez Martinez, M., York, D., Hall, C.M. and Hanes, J.A., 1984. Oldest reliable ^{40}Ar/^{39}Ar ages for terrestrial rocks: Barberton Mountain komatiites. Nature, 307: 352-354.

Lowe, D.R., 1994. Accretionary history of the Archaean Barberton greenstone belt (3.55-3.22 Ga), South Africa. Geology, 22: 1099-1102.

Lowe, D.R., 1999. Geologic evolution of the Barberton greenstone belt and vicinity. In: D.R. Lowe and G.R. Byerly (Eds.), Geologic Evolution of the Barberton Greenstone Belt, South Africa. Spec.Paper Geol. Soc. Amer., 329: 287-312.

Lowe, D. R. and Byerly, G.R., 1999. Stratigraphy of the west-central part of the Barberton greenstone belt, South Africa. In: D.R. Lowe and G.R. Byerly (Eds.), Geologic Evolution of the Barberton Greenstone Belt, South Africa. Spec. Paper Geol. Soc. Amer., 329: 1-36.

Ludwig, K.R., 1993. A computer program for processing Pb-U-Th isotope data, version 1.24, Denver. Open File Rep. U.S. Geol. Surv., 88-542: 32pp.

Ludwig, K.R., 2000. Isoplot/Ex : a geochronological toolkit for Microsoft Excel. Berkeley Geochronology Center, Berkeley, California.

Morimoto, N., 1988. Nomenclature of pyroxenes. Mineral. Mag., 52: 535-550.

Mukhopadhyay, A., Bhattacharya, A. and Mohanty, L., 1992. Geobarometers involving clinopyroxene, garnet, plagioclase, ilmenite, rutile, sphene and quartz: estimation of pressure in quartz-absent assemblages. Contrib. Mineral. Petrol., 110: 346-354.

Paces, J.B. and Miller Jr., J.D., 1993. Precise U-Pb ages of Duluth Complex and related mafic intrusions, northeastern Minnesota: geochronological insights to physical, petrogenetic, paleomagnetic and tectonomagmatic processes associated with the 1.1 Ga Midcontinent Rift System. J. Geophys. Res., B98: 13997-14013.

Petö, P., 1976. An experimental investigation of melting relations involving muscovite and paragonite in the silica-saturated portion of the system K_2O-Na_2O-Al_2O_3-SiO_2-H_2O to 15 kbar total pressure. Prog. in Exper. Petrol., NERC London, 3rd Rep. : 41-45.

Poller, U., Liebetrau, V. and Todt, W., 1997. U-Pb single-zircon dating under cathodoluminescence control (CLC-method): application to polymetamorphic orthogneisses. Chem. Geol., 139: 287-297.

Powell, R., 1985. Regression diagnostics and robust regression in geothermometer/geobarometer calibration: the garnet-clinopyroxene geothermometer revisited. J. Metamorphic Geol., 2: 33-42.

Powell, R. and Holland, T.J.B., 1988. An internally consistent dataset with uncertainties and correlations: 3. Applications to geobarometry, worked examples and a computer program. J Metamorphic Geol., 6: 173-204.

Robb, L. J., 1983a. Geological and chemical characteristics of late granite plutons in the Barberton region and Swaziland with an emphasis on the Dalmein pluton a review. Spec. Publ. Geol. Soc. S. Afr., 9: 153-167.

Robb, L.J., 1983b. The nature, origin and significance of Archaean migmatites in the Barberton Mountain Land: a new approach in the assessment of early crustal evolution. Spec. Publ. Geol. Soc.S. Afr., 9: 81-101.

Robb, L.J. and Anhaeusser, C. R., 1983. Chemical and petrogenetic characteristics of Archaean tonalite-trondhjemite gneiss plutons in the Barberton Mountain Land. Spec. Publ. Geol. Soc. S. Afr., 9: 103-116.

Robb, L. J., Anhaeusser, C. R. and van Nierop, D. A., 1983. The recognition of the Nelspruit batholith north of the Barberton greenstone belt and its significance in terms of Archaean crustal evolution. Spec. Publ. Geol. Soc. S. Afr., 9: 117-130.

Spear, F.S., 1988. Metamorphic fractional crystallisation and internal metasomatism by diffusional homogenization of zoned garnets. Contrib. Mineral. Petrol., 99: 507-517.

Spear, F.S., 1993. Metamorphic phase equilibria and pressure-temperature-time path. Monograph, Mineral. Soc. Amer., 799pp.

Spear, F.S., Kohn, M.J., Florence, F.P. and Menard, T., 1991. A model for garnet and plagioclase growth in pelitic schists: implications for thermobarometry and P-T path determinations. J. Metamorphic Geol., 8: 683-696.

Stacey, J.S. and Kramers, J.D., 1975. Approximation of terrestrial lead isotope evolution by a two stage model. Earth Planet. Sci. Lett., 26: 207-221.

Stevens, G., Droop, G.T.R., Armstrong, R.A. and Anhaeusser, C. R., (in prep.). The Schapenburg schist belt: amphibolite facies metamorphism in Fig Tree Group metasediments as a consequence of *c*.3.23 Ga terrane accretion in the Barberton greenstone belt, South Africa (to be submitted to J. Metamorphic Geol.).

Tegtmeyer, A.R. and Kröner, A., 1987. U-Pb zircon ages bearing on the nature of early Archaean greenstone belt evolution, Barberton Mountainland, southern Africa. Precambrian Res., 36: 1-20.

Viljoen, M.J. and Viljoen, R.P., 1969. An introduction to the geology of the Barberton granite-greenstone terrain. Spec. Publ. Geol. Soc. S. Afr., 2: 9-28.

Viljoen, R. P., Saager, R. and Viljoen, M. J., 1969. Metallogenesis and ore control in the Steynsdorp Goldfield Barberton Mountain Land, South Africa. Econ. Geol., 64: 778-797.

Williams, I.S. and Claesson, S., 1987. Isotopic evidence for the Precambrian provenance and

Caledonian metamorphism of high grade paragneisses from the Seve Nappes, Scandinavian Caledonides. II. Ion microprobe zircon U-Th-Pb. Contrib. Mineral. Petrol., 97: 205-217.

Witt-Eickschen, G. and Seck, H.A., 1991. Solubility of Ca and Al in orthopyroxene from spinel peridotite: an improved version of an empirical geothermometer. Contrib. Mineral. Petrol., 106: 431-439.

Xie, X., Byerly, G.R. and Ferrell, R.E., Jr., 1997. IIb trioctahedral chlorite from the Barberton greenstone belt; crystal structure and rock composition constraints with implications to geothermometry. Contrib. Mineral. Petrol., 126 (3): 275-291.

_____**oOo**_____